ON-POLICY MODEL ERRORS IN REINFORCEMENT LEARNING

Anonymous authors
Paper under double-blind review

ABSTRACT

Model-free reinforcement learning algorithms can compute policy gradients given sampled environment transitions, but require large amounts of data. In contrast, model-based methods can use the learned model to generate new data, but model-errors and biases can render learning unstable or sub-optimal. In this paper, we present a novel method that combines real-world data and a learned model in order to get the best of both worlds. The core idea is to exploit the real-world data for on-policy predictions and use the learned model only to generalize to different actions. Specifically, we use the data as time-dependent on-policy correction terms on top of a learned model, to retain the ability to generate data without accumulating errors over long prediction horizons. We motivate this method theoretically and show that it counteracts an error term for model-based policy improvement. Experiments on MuJoCo- and PyBullet-benchmarks show that our method can drastically improve existing model-based approaches without introducing additional tuning parameters.

1 INTRODUCTION

Model-free reinforcement learning (RL) has made great advancements in diverse domains such as single- and multi-agent game play (Mnih et al., 2015; Silver et al., 2016; Vinyals et al., 2019), robotics (Kalashnikov et al., 2018) or neural architecture search (Zoph & Le, 2016). All of these model-free approaches rely on large amounts of interactions with the environment to ensure successful learning. While this issue is less severe for environments that can easily be simulated, it limits the applicability of model-free RL to (real-world) domains where data is scarce.

Model-based RL (MBRL) aims to reduce the amount of data required for policy optimization by learning a model that approximates the true environment, which we can use to generate cheap, simulated state transitions (Sutton, 1990; Racanière et al., 2017; Moerland et al., 2020). While early approaches on low-dimensional tasks by Schneider (1997); Deisenroth & Rasmussen (2011) used probabilistic models with closed-form posteriors, recent methods rely on (Bayesian) neural networks to scale to more complex tasks on discrete (Kaiser et al., 2019) and continuous (Chua et al., 2018; Kurutach et al., 2018) action spaces. However, the learned representation of the true environment always remains imperfect and as such introduces an error source to the RL problem (Atkeson & Santamaria, 1997; Abbeel et al., 2006). Hence, a key challenge in MBRL is *model-bias*; small errors in the learned models that can compound over multi-step predictions and lead to lower asymptotic performance in contrast to model-free approaches.

To address these challenges with both model-free and model-based RL, Levine & Koltun (2013); Chebotar et al. (2017) propose to combine the merits of both. While there are multiple possibilities to combine the two methodologies, in this work we focus on improving the model's predictive state distribution such that it more closely resembles the true environment.

Contributions The main contribution of this paper are on-policy corrections (OPC), a novel hyperparameter-free methodology that uses on-policy transition data on top of a separately learned model to enable accurate long-term predictions for MBRL. A key strength of our approach is that it does not introduce any new parameters that need to be hand-tuned for specific tasks. We theoretically motivate our approach by means of a policy improvement bound and show that we can recover the true state distribution when generating trajectories on-policy with the model. We illustrate how OPC improves the quality of policy gradient estimates in a simple toy example and evaluate it on various continuous control tasks from the MuJoCo control suite and their PyBullet variants. There, we

demonstrate that OPC improves current state-of-the-art MBRL algorithms in terms of data efficiency, especially for the more difficult PyBullet environments.

Related Work To counteract model-bias, several approaches combine ideas from model-free and model-based RL. For example, Levine & Koltun (2013) guide a model-free algorithm via model-based planning towards promising regions in the state space, Kalweit & Boedecker (2017) augment the training data by an adaptive ratio of simulated transitions, Talvitie (2017) use 'hallucinated' transition tuples from simulated to observed states as to self-correct the model, and Feinberg et al. (2018); Buckman et al. (2018) use a learned model to improve the value function estimate. Janner et al. (2019) use the learned model only for short simulated rollouts starting from real observed states to mitigate the issue of compounding errors for long term predictions. Cheng et al. (2019) extend first-order model-free algorithms via adversarial online learning to leverage prediction models in a regret-optimal manner. Instead of adding simulated transitions to the training data, Clavera et al. (2020) employ a model to augment an actor-critic objective, which they optimize via back-propagation through time; adapting the planning horizon interpolates between a pure model-based and model-free approach. A downside of most existing approaches is that they introduce additional hyperparameters that are critical to the learning performance (Zhang et al., 2021).

In addition to empirical performance, recent work builds on the theoretical guarantees for model-free approaches by Kakade & Langford (2002); Schulman et al. (2015) to provide guarantees for MBRL. Luo et al. (2018) provide a general framework to show monotonic improvement towards a local optimum of the value function, while Janner et al. (2019) present a lower-bound on performance for different rollout schemes and horizon lengths. Yu et al. (2020) show guaranteed improvement in the offline MBRL setting by augmenting the reward with an uncertainty penalty, while Clavera et al. (2020) present improvement guarantees in terms of the model's and value function's gradient errors.

A related field to MBRL that also combines models with data for learning is iterative learning control (ILC) (Bristow et al., 2006). The differences between the two are the following: RL typically focuses on finding parametric feedback policies for general reward functions, whereas ILC seeks an open-loop sequence of actions with fixed length to improve state tracking performance. Further, the model in ILC is often derived from first principles and then kept fixed, whereas in MBRL the model is continuously improved upon new data. Closest related to RL and our approach is optimization-based ILC (Owens & Hätönen, 2005; Schöllig & D'Andrea, 2009; Mishra et al., 2010), in which an (approximate) linear dynamics model is used to guide the search for optimal actions. Recently, Baumgärtner & Diehl (2020) extended the ILC setting to nonlinear dynamics and more general reward signals.

Little work is available that draws connections between RL and ILC (Zhang et al., 2019) with one notable exception: Abbeel et al. (2006) use the observed data from the last rollout to account for a mismatch in the dynamics model. The limitations of this approach are that deterministic dynamics are assumed, the policy optimization itself requires a line search procedure with rollouts on the true environment and that it was not combined with model learning. We build on this idea and extend it to the stochastic setting of MBRL by making use of recent advances in RL and model learning.

2 Problem Statement and Background

We consider the Markov decision process (MDP) $(\mathcal{S}, \mathcal{A}, p, r, \gamma, \rho)$ where $\mathcal{S} \subseteq \mathbb{R}^{|\mathcal{S}|}$ and $\mathcal{A} \subseteq \mathbb{R}^{|\mathcal{A}|}$ are the continuous state and action spaces, respectively. The unknown environment dynamics are described by the transition probability $p(\mathbf{s}_{t+1} \mid \mathbf{s}_t, \mathbf{a}_t)$, an initial state distribution $\rho(\mathbf{s}_0)$ and the reward signal $r(\mathbf{s}, \mathbf{a})$. The goal in RL is to find a policy $\pi_\theta(\mathbf{a}_t \mid \mathbf{s}_t; \theta)$ parameterized by θ that maximizes the expected return, discounted by $\gamma \in [0, 1]$ over episodes of length T,

$$\eta_\pi = \mathop{\mathbb{E}}_{\mathbf{s}_{0:T}, \mathbf{a}_{0:T}} \left[\sum\nolimits_{t=0}^{T} \gamma^t r(\mathbf{s}_t, \mathbf{a}_t) \right], \quad \mathbf{s}_{t+1} \sim p(\mathbf{s}_{t+1} \mid \mathbf{s}_t, \mathbf{a}_t), \quad \mathbf{s}_0 \sim \rho, \quad \mathbf{a}_t \sim \pi_\theta(\mathbf{s}_t). \tag{1}$$

The expectation is taken with respect to the trajectory under the stochastic policy π_θ starting from some stochastic initial state. Direct maximization of Eq. (1) is challenging, since we do not know the environment's transition probabilities p. In MBRL, we learn a model for the transitions and reward function from data, $\tilde{p}(\mathbf{s}_{t+1} \mid \mathbf{s}_t, \mathbf{a}_t) \approx p(\mathbf{s}_{t+1} \mid \mathbf{s}_t, \mathbf{a}_t)$ and $\tilde{r}$ respectively, and subsequently solve

$$\max_\theta \tilde{\eta}_\pi = \max_\theta \mathop{\mathbb{E}}_{\mathbf{s}_{0:T}, \mathbf{a}_{0:T}} \left[\sum\nolimits_{t=0}^{T} \gamma^t \tilde{r}(\mathbf{s}_t, \mathbf{a}_t) \right], \quad \mathbf{s}_{t+1} \sim \tilde{p}(\mathbf{s}_{t+1} \mid \mathbf{s}_t, \mathbf{a}_t), \quad \mathbf{s}_0 \sim \rho, \quad \mathbf{a}_t \sim \pi_\theta(\mathbf{s}_t). \tag{2}$$

Algorithm 1 General Model-based Reinforcement Learning

1: **for** $n = 1, \dots$ **do**
2: Rollout policy π_n on the environment and store transitions $\mathcal{D}_n = \{(\hat{\mathbf{s}}_t^n, \hat{\mathbf{a}}_t^n, \hat{\mathbf{s}}_{t+1}^n)\}_{t=0}^{T-1}$
3: $\tilde{p}_n(\mathbf{s}_{t+1} \mid \mathbf{s}_t, \mathbf{a}_t)$: Learn a global dynamics model given all data $\mathcal{D}_{1:n} = \bigcup_{b=1}^{n} \mathcal{D}_b$
4: $\theta_{n+1} = \theta_n + \alpha \nabla \tilde{\eta}_{\pi_n}$: Optimize the policy based on the model $\tilde{p}$ with any RL algorithm

as a surrogate problem for Eq. (1). The choice of initial state distribution $\tilde{\rho}(\mathbf{s}_0)$ depends on the optimization method: For model predictive control, Chua et al. (2018) use the current state to optimize the next action based on a rollout, while Janner et al. (2019) use the empirical state distribution observed from the true environment. In the following we focus on the latter and, for ease of exposition, assume a known reward function $\tilde{r} = r$ even though we learn it jointly with p in our experiments.

In the following, we use π_n and η_n to denote the policy and its performance based on the parameters θ_n at iteration n. The 'hat'-notation for states and actions refers to observed quantities from the true environment. Algorithm 1 summarizes the overall procedure for MBRL: At each iteration n we store the transition tuples $\mathcal{D}_n = \{(\hat{\mathbf{s}}_t^n, \hat{\mathbf{a}}_t^n, \hat{\mathbf{s}}_{t+1}^n)\}_{t=0}^{T-1}$ obtained by rolling out the current policy π_n on the real environment in Line 2, approximate the environment with a learned model $\tilde{p}_n(\mathbf{s}_{t+1} \mid \mathbf{s}_t, \mathbf{a}_t)$ based on the data in Line 3, and optimize the policy based on the proxy objective in Eq. (2) in Line 4.

Model Choices The choice of model $\tilde{p}$ plays a key role, since it defines the surrogate problem Eq. (2). Inside the optimization loop, the model is typically used to predict sequences of transitions τ with length H. One common option is to use a purely data-based model in form of a replay buffer that replays past transitions from a given trajectory b starting at time step t,

$$\tilde{p}^{\text{replay}}(\tau_{t:t+H} \mid t, b) = \prod_{t'=t}^{t+H} \tilde{p}^{\text{replay}}(\hat{\mathbf{s}}_{t'} \mid t', b) \quad \text{with} \quad \tilde{p}^{\text{replay}}(\hat{\mathbf{s}}_t \mid t, b) = \delta(\mathbf{s}_t - \hat{\mathbf{s}}_t^b) \tag{3}$$

where $\delta(\cdot)$ denotes a Dirac-delta distribution and the trajectory index b is typically chosen uniformly at random from the last few trajectories, $n - B < b \leq n$ based on a replay buffer of size B. An alternative is to instead summarize all the past data $\mathcal{D}_{1:n} = \cup_{b=1}^{n} \mathcal{D}_b$ in a parametric model coming from a distribution family $\mathcal{P}$ by maximizing the marginal log-likelihood $\mathcal{L}$,

$$\tilde{p}^{\text{model}}(\mathbf{s}_{t+1} \mid \mathbf{s}_t, \mathbf{a}_t) = \operatorname*{arg\,max}_{\tilde{p} \in \mathcal{P}} \sum_{(\hat{\mathbf{s}}_t, \hat{\mathbf{a}}_t, \hat{\mathbf{s}}_{t+1}) \in \mathcal{D}_{1:n}} \mathcal{L}(\hat{\mathbf{s}}_{t+1}; \hat{\mathbf{s}}_t, \hat{\mathbf{a}}_t), \tag{4}$$

which for each state-action pair $(\mathbf{s}_t, \mathbf{a}_t)$ models a distribution over the next state $\mathbf{s}_{t+1}$, such that $\tilde{p}^{\text{model}}(\tau_{t:t+H} \mid t, b) = \delta(\mathbf{s}_t - \hat{\mathbf{s}}_t^b) \prod_{t'=t}^{t+H-1} \tilde{p}^{\text{model}}(\mathbf{s}_{t'+1} \mid \mathbf{s}_{t'}, \mathbf{a}_{t'})$ with $\mathbf{a}_{t'} \sim \pi_\theta$. For both models we can sample H-step predictions by first sampling a replay buffer index $b \sim \text{Categorical}(\{n+1-B, \dots, n\})$ and then rolling out following the respective state sequence distributions $\tilde{p}(\tau_{t:t+H} \mid t, b)$.

3 On-policy Corrections

In this section, we analyze how the choice of model impacts policy improvement, develop OPC as a model that can eliminate one term in the improvement bound, and analyze its properties.

3.1 Policy Improvement

Independent of whether we use a replay buffer Eq. (3) or summarize the data in a world model Eq. (4), our goal is to find an optimal policy that maximizes Eq. (1) via the corresponding model-based proxy objective Eq. (2). To this end, we would like to know how a policy improvement $\tilde{\eta}_{n+1} - \tilde{\eta}_n \geq 0$ based on the model $\tilde{p}$, which is what we optimize in Eq. (2), relates to the true gain in performance $\eta_{n+1} - \eta_n$ on the environment with unknown dynamics p. While the two are equal without model errors, $\tilde{p} = p$, in general the larger the model error, the worse we can expect our proxy objective to be. More concretely, we show in Appendix A.1 that the policy improvement can be decomposed as

$$\underbrace{\eta_{n+1} - \eta_n}_{\text{True policy improvement}} \geq \underbrace{\tilde{\eta}_{n+1} - \tilde{\eta}_n}_{\text{Model policy improvement}} - \underbrace{|\eta_{n+1} - \tilde{\eta}_{n+1}|}_{\text{Off-policy model error}} - \underbrace{|\eta_n - \tilde{\eta}_n|}_{\text{On-policy model error}}, \tag{5}$$

where a performance improvement on our model-based objective in Eq. (2) only translates to a gain in Eq. (1) if two error terms are sufficiently small. These terms depend on how good the performance estimate based on our model, $\tilde{\eta}$, matches the true performance, η. If the reward function is known, this term only depends on the model quality of $\tilde{p}$ relative to p. Note that in contrast to the result by Janner et al. (2019), Eq. (5) is a bound on the policy improvement instead of a lower bound on η_{n+1}.

The first error term compares η_{n+1} and $\tilde{\eta}_{n+1}$, the performance estimation gap under the optimized policy π_{n+1} that we obtain in Line 4 of Algorithm 1. Since at this point we have only collected data with π_n in Line 2, this term depends on the generalization properties of our model to new data; what we call the *off-policy model error*. For our data-based model $\tilde{p}^{\text{replay}}$ that just replays data under π_n independently of the action, this term can be bounded for stochastic policies. For example, Schulman et al. (2015) bound it by the average KL-divergence between π_n and π_{n+1}. For learned models $\tilde{p}^{\text{model}}$, it depends on the generalization properties of the model (Luo et al., 2018; Yu et al., 2020). While understanding model generalization better is an interesting research direction, we will assume that our learned model generalizes to new actions somewhat reasonably in the following.

While the first term hinges on model-generalization, the second term is the *on-policy model error*, i.e., the deviation between η_n and $\tilde{\eta}_n$ under the current policy π_n. This error term goes to zero for $\tilde{p}^{\text{replay}}$ as we use more data $B \to \infty$ and if we do not update our policy, since the transition data are sampled on-policy from the true environment and the mean converges, c.f., Appendix A.2. While the learned model is also trained with on-policy data, small errors in our model compound as we iteratively predict ahead in time. Consequently, for prediction horizons shorter than the effective horizon encoded in the discount factor, $H < \gamma/(1-\gamma)$, the on-policy error term grows as $\mathcal{O}(\min(H/(1-\gamma), H^2))$, c.f., (Janner et al., 2019) and Appendix A.3. The root cause is the same as in behavior cloning (Ross & Bagnell, 2010, Theorem 2.1), where small errors aggregate over time.

3.2 Combining Learned Models and Replay Buffer

The key insight of this paper is that the replay buffer in Eq. (3) and the parametric model in Eq. (4) have opposing strengths: The replay buffer has low error on-policy, but high error off-policy since it replays transitions from past data, i.e., they are independent of the actions chosen under the new policy. In contrast, the learned model can generalize to new actions by extrapolating from the data and thus has lower error off-policy, but errors compound over the prediction horizon H.

An ideal model would combine the model-free and model-based approaches in a way such that it retains the unbiasedness of on-policy generated data, but also generalizes to new policies via the model. To this end, we propose to adjust the replay buffer's prediction by an offset that accounts for the model predictions given a new state-action pair. In particular, we use the model's mean prediction $\tilde{f}(\mathbf{s}_t, \mathbf{a}_t) = \mathbb{E}_{\mathbf{s}_{t+1}}[\tilde{p}^{\text{model}}(\mathbf{s}_{t+1} \mid \mathbf{s}_t, \mathbf{a}_t)]$ to construct the joint model

$$\tilde{p}^{\text{opc}}(\mathbf{s}_{t+1} \mid \mathbf{s}_t, \mathbf{a}_t, b) = \underbrace{\delta\big(\mathbf{s}_{t+1} - \hat{\mathbf{s}}^b_{t+1}\big)}_{\tilde{p}^{\text{replay}}(\mathbf{s}_{t+1} \mid t+1, b)} * \underbrace{\delta\big(\mathbf{s}_{t+1} - \big[\tilde{f}(\mathbf{s}_t, \mathbf{a}_t) - \tilde{f}(\hat{\mathbf{s}}^b_t, \hat{\mathbf{a}}^b_t)\big]\big)}_{\text{Model mean correction to generalize to } \mathbf{s}_t,\, \mathbf{a}_t}, \tag{6}$$

where $*$ denotes the convolution of the two distributions and b refers to a specific rollout stored in the replay buffer that was observed on the true environment. Given a batch-index b, the OPC model in Eq. (6) transitions deterministically according $\mathbf{s}_{t+1} = \hat{\mathbf{s}}^b_{t+1} + \tilde{f}(\mathbf{s}_t, \mathbf{a}_t) - \tilde{f}(\hat{\mathbf{s}}^b_t, \hat{\mathbf{a}}^b_t)$, resembling the equations in ILC (c.f., Baumgärtner & Diehl (2020) and Appendix D). If we rollout $\tilde{p}^{\text{opc}}$ along a trajectory, starting from a state $\hat{\mathbf{s}}^b_t$ and apply the recorded actions from the replay buffer, $\hat{\mathbf{a}}^b_t$, the correction term in the right of Eq. (6) cancels out and we have $\tilde{p}^{\text{opc}}(\mathbf{s}_{t+1} \mid \hat{\mathbf{s}}^b_t, \hat{\mathbf{a}}^b_t, b) = \tilde{p}^{\text{replay}}(\mathbf{s}_{t+1} \mid t+1, b) = \delta(\mathbf{s}_{t+1} - \hat{\mathbf{s}}^b_{t+1})$. Thus OPC retrieves the true on-policy data distribution independent of the prediction quality of the model, which is why we refer to this method as *on-policy corrections* (OPC). This behaviour is illustrated in Fig. 1a, where even though the model (blue) is biased on-policy, OPC corrects the model's prediction to match the true data. In Fig. 1b, we show how this affects predicted rollouts on a simple stochastic double-integrator environment. Even though small on-policy errors in $\tilde{p}^{\text{model}}$ (blue) compound over time, the corresponding $\tilde{p}^{\text{opc}}$ matches the ground-truth environment data closely. Note that even though the model in Eq. (6) is deterministic, we retain the environment's stochasticity from the data in the transitions to $\hat{\mathbf{s}}_{t+1}$, so that we recover the on-policy aleatoric uncertainty (noise) from sampling different indexes b (different reference trajectories).

When we apply actions different from $\hat{\mathbf{a}}^b_t$ (off-policy), $\tilde{p}^{\text{opc}}$ still uses the data from the replay buffer, but the correction term in Eq. (6) uses the learned model to predict how the next state *changes* in

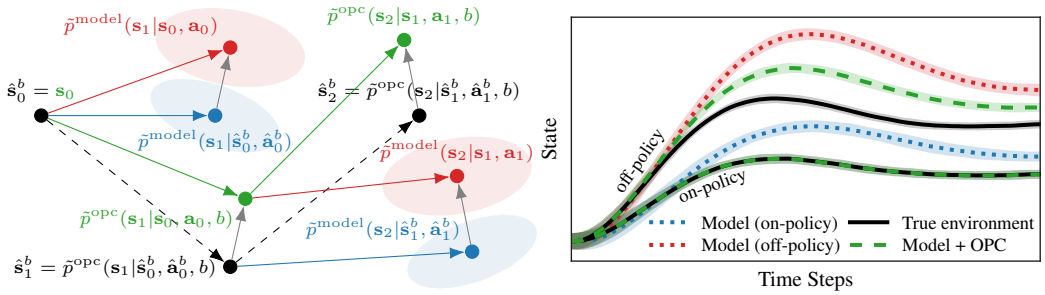

(a) Multi-step predictions with OPC.

(b) State distribution over time.

Figure 1: Illustration to compare predictions of the three models Eqs. (3), (4) and (6) starting from the same state $\hat{\mathbf{s}}_0^b$. In Fig. 1a, we see that on-policy, i.e., using actions $(\hat{\mathbf{a}}_0^b, \hat{\mathbf{a}}_1^b)$, $\tilde{p}^{\text{replay}}$ returns environment data, while $\tilde{p}^{\text{model}}$ (blue) is biased. We correct this on-policy bias in expectation to obtain $\tilde{p}^{\text{opc}}$. This allows us to retain the true state distribution when predicting with these models recursively (c.f., bottom three lines in Fig. 1b). When using OPC for off-policy actions $(\mathbf{a}_0, \mathbf{a}_1)$, $\tilde{p}^{\text{opc}}$ does not recover the true off-policy state distribution since it relies on the biased model. However, the corrections generalize locally and reduce prediction errors in Fig. 1b (top three lines).

expectation relative to the prediction under $\hat{\mathbf{a}}_t^b$. That is, in Fig. 1a for a new $\mathbf{a}_t$ the model predicts the state distribution show in red. Correspondingly, we shift the static prediction $\hat{\mathbf{s}}_{t+1}^b$ by the difference in means (gray arrow) between the two predictions; i.e., the *change in trajectory* by changing from $\hat{\mathbf{a}}_t^b$ to $\mathbf{a}_t$. Since we shift the model predictions by a time-dependent but constant offset, this does not recover the true state distribution unless the model has zero error. However, regardless it can help with long-term predictions in Fig. 1b by shifting the model off-policy predictions (red) to the OPC predictions (green), which are closer to the state distribution of our environment under the new policy.

3.3 Theoretical Analysis

As mentioned in the previous sections, OPC is motivated as to reduce the on-policy model error from Eq. (5) to tighten the improvement bound. In this section, we analyze this performance gap from a theoretical perspective and show that with OPC, the on-policy model error is minimized and independent of the learned model's error. To this end, we derive a more general form of the predictive model for OPC Eq. (6) where we consider $\hat{\mathbf{s}}_{t+1}^b$ as a random variable following the true environment's transition dynamics instead of treating it as an observed quantity. While impossible to implement in practice, this formulation helps for the theoretical analysis. The generalized OPC-model is defined as

$$\tilde{p}_\star^{\text{opc}}(\mathbf{s}_{t+1} \mid \mathbf{s}_t, \mathbf{a}_t, b) = \underbrace{p(\hat{\mathbf{s}}_{t+1} \mid \hat{\mathbf{s}}_t^b, \hat{\mathbf{a}}_t^b)}_{\text{On-policy transition}} * \underbrace{\delta\Big(\mathbf{s}_{t+1} - \Big[\tilde{f}(\mathbf{s}_t, \mathbf{a}_t) - \tilde{f}(\hat{\mathbf{s}}_t^b, \hat{\mathbf{a}}_t^b)\Big]\Big)}_{\text{Mean correction term}}, \tag{7}$$

which highlights that it transitions according to the true on-policy dynamics conditioned on data from the replay buffer, combined with a correction term. We provide a detailed derivation for the generalized model in Appendix A. With Eq. (7), we have the following result:

Theorem 1. *Let $\tilde{\eta}_\star^{\text{opc}}$ and η be the expected return under the generalized* OPC*-model Eq.* (7) *and the true environment, respectively. Assume that the learned model's mean transition function $\tilde{f}(\mathbf{s}_t, \mathbf{a}_t) = \mathbb{E}[\tilde{p}^{\text{model}}(\mathbf{s}_{t+1} \mid \mathbf{s}_t, \mathbf{a}_t)]$ is L_f-Lipschitz and the reward $r(\mathbf{s}_t, \mathbf{a}_t)$ is L_r-Lipschitz. Further, if the policy $\pi(\mathbf{a}_t \mid \mathbf{s}_t)$ is L_π-Lipschitz with respect to $\mathbf{s}_t$ under the Wasserstein distance and its (co-)variance $\text{Var}[\pi(\mathbf{a}_t \mid \mathbf{s}_t)] = \Sigma_\pi(\mathbf{s}_t) \in \mathbb{S}_+^{|\mathcal{A}|}$ is finite over the complete state space, i.e., $\max_{\mathbf{s}_t \in \mathcal{S}} \text{trace}\{\Sigma_\pi(\mathbf{s}_t)\} \leq \bar{\sigma}_\pi^2$, then with $C_1 = \sqrt{2(1 + L_\pi^2)} L_f L_r$ and $C_2 = \sqrt{L_f^2 + L_\pi^2}$*

$$|\eta - \tilde{\eta}_\star^{\text{opc}}| \leq \frac{C_1}{1 - \gamma} |\mathcal{A}|^{\frac{1}{4}} C_2^T \sqrt{T} \bar{\sigma}_\pi. \tag{8}$$

We provide a proof in Appendix A. From Theorem 1, we can observe the key property of OPC: for deterministic policies, the on-policy model error from Eq. (5) is zero and independent of the learned

models' predictive distribution $\tilde{p}^{\text{model}}$, so that $\eta = \tilde{\eta}_\star^{\text{opc}}$. For policies with non-zero variance, the bound scales exponentially with T, highlighting the problem of compounding errors. In this case, as in the off-policy case, the model quality determines how well we can generalize to different actions. To alleviate this issue, one could extend Theorem 1 similar to the results in Janner et al. (2019) such that the rollouts are only of length $H \ll T$.

In practice, $\tilde{p}_\star^{\text{opc}}$ can never be realized as it requires the true (unknown) state distribution. However, we can approximate it by $\tilde{p}^{\text{opc}}$ Eq. (6) using an ever-increasing size of reference trajectories such that the on-policy error converges to zero in probability.

Lemma 1. *Let M be a MDP with dynamics $p(\mathbf{s}_{t+1} \mid \mathbf{s}_t, \mathbf{a}_t)$ and reward $r < r_{\max}$. Let $\tilde{M}$ be another MDP with dynamics $\tilde{p}^{\text{model}} \neq p$. Assume a deterministic policy $\pi : \mathcal{S} \mapsto \mathcal{A}$ and a set of trajectories $\mathcal{D} = \bigcup_{b=1}^{B} \{(\hat{\mathbf{s}}_t^b, \hat{\mathbf{a}}_t^b, \hat{\mathbf{s}}_{t+1}^b)\}_{t=0}^{T-1}$ collected from M under π. If we use* OPC *Eq.* (6) *with data $\mathcal{D}$, then*

$$\lim_{B\to\infty} \Pr\left(|\eta - \tilde{\eta}^{\text{opc}}| > \varepsilon\right) = 0 \quad \forall \varepsilon \quad \textit{with convergence rate} \quad \mathcal{O}(1/B). \tag{9}$$

We provide a proof in Appendix A. Lemma 1 states that given sufficient reference on-policy data, the performance gap due to model errors becomes arbitrarily small for *any* model $\tilde{p}^{\text{model}}$ when using OPC. While the assumption for infinite on-policy data in Lemma 1 is unrealistic for practical applications, we found empirically that OPC drastically reduces the on-policy model error even when the assumptions are violated. In our implementation, we use stochastic policies as well as trajectories from previous policies, i.e., off-policy data, for the corrections in OPC (see also Section 4.2).

3.4 Discussion

Epistemic uncertainty So far we have only considered aleatoric uncertainty (noise) in our transition models. In practice, modern methods additionally distinguish epistemic uncertainty that arises from having seen limited data (Deisenroth & Rasmussen, 2011; Chua et al., 2018). This leads to a distribution (or an ensemble) of models, where each sample could explain the data. In this setting, we apply OPC by correcting *each sample individually*. This allows us to retain epistemic uncertainty estimates after applying OPC.

Limitations Since OPC uses on-policy data, it is inherently limited to local policy optimization where the policy changes slowly over time. As a consequence, it cannot be applied with global exploration schemes like the one proposed by Curi et al. (2020). Similarly, since OPC uses the replay buffer data and corrects it only with the expected learned model, $\tilde{p}^{\text{opc}}$ always uses the on-policy transition noise (aleatoric uncertainty) from the data, even if the model has learned to represent it. While not having to learn a representation for aleatoric uncertainty can be a strength, it limits our approach to environments where the aleatoric uncertainty does not vary significantly with state/actions. While it is possible to extend the method to heteroscedastic noise setting, this requires distinguishing model error from transition noise as in (Schöllig & D'Andrea, 2009), which generally requires additional assumptions. Lastly, our method applies directly only to MDPs, since we rely on state-observations. Extending the ideas to partially-observed environments is an interesting direction for future research.

4 Experimental Results

We begin the experimental section with a motivating example on a toy problem to highlight the impact of OPC on the policy gradient estimates in the presence of model errors. The remainder of the section focuses on comparative evaluations and ablation studies on complex continuous-control tasks.

4.1 Illustrative Example

In Section 3.3 we investigate the influence of the model error directly on the expected return from a theoretical perspective. From a practical standpoint, another relevant question is how the policy optimization and the respective policy gradients are influenced by model errors. For general environments and reward signals, this question is difficult to answer, due to the typically high-dimensional state/action spaces and large number of parameters governing the dynamics model as well as the policy. To shed light on this open question, we resort to a simple low-dimensional example and investigate how OPC improves the gradient estimates under a misspecified dynamics model.

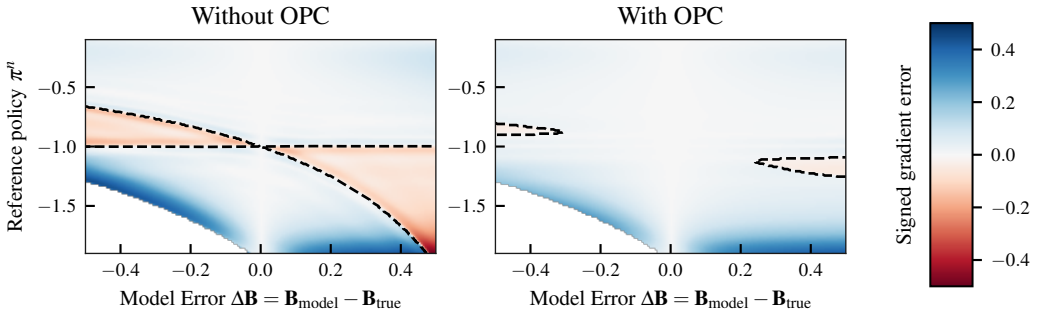

Figure 2: Signed gradient error when using inaccurate models Eq. (10) to estimate the policy gradient without (left) and with (right) OPC. The background's opacity depicts the error's magnitude, whereas color denotes if the sign of estimated and true gradient differ (red) or coincide (blue). OPC improves the gradient estimate in the presence of model errors. Note that the optimal policy is $\theta^* = -1.0$.

In particular, we assume a one-dimensional deterministic environment with linear transitions and a linear policy. The benefits of this example are that we can 1) compute the true policy gradient based on a single rollout (determinism), 2) determine the environment's closed-loop stability under the policy (linearity), 3) and visualize the gradient error as a function of all relevant parameters (low dimensionality). The dynamics and initial state distribution are specified by $p(\mathbf{s}_{t+1} \mid \mathbf{s}_t, \mathbf{a}_t) = \delta(\mathbf{A}\mathbf{s}_t + \mathbf{B}\mathbf{a}_t \mid \mathbf{s}_t, \mathbf{a}_t)$ with $\rho(\mathbf{s}_0) = \delta(\mathbf{s}_0)$ where $\mathbf{A}, \mathbf{B} \in \mathbb{R}$ and $\delta(\cdot)$ denotes the Dirac-delta distribution. We define a deterministic linear policy $\pi_\theta(\mathbf{a}_t \mid \mathbf{s}_t) = \delta(\theta \mathbf{s}_t \mid \mathbf{s}_t)$ that is parameterized by the scalar $\theta \in \mathbb{R}$. The objective is to drive the state to zero, which we encode with an exponential reward $r(\mathbf{s}_t, \mathbf{a}_t) = \exp\left\{-(\mathbf{s}_t/\sigma_r)^2\right\}$. Further, we assume an approximate dynamics model

$$\tilde{p}(\mathbf{s}_{t+1} \mid \mathbf{s}_t, \mathbf{a}_t) = \delta((\mathbf{A} + \Delta\mathbf{A})\mathbf{s}_t + (\mathbf{B} + \Delta\mathbf{B})\mathbf{a}_t \mid \mathbf{s}_t, \mathbf{a}_t), \tag{10}$$

where $\Delta\mathbf{A}, \Delta\mathbf{B}$ quantify the mismatch between the approximate model and the true environment. In practice, the mismatch can arise due to noise-corrupted observations of the true state or, in the case of stochastic environments, due to finite amount of training data.

With the setting outlined above, we investigate how model errors influence the estimation of policy gradients. To this end, we roll out different policies under approximate models with varying degree of error $\Delta\mathbf{B}$. For each policy/model combination, we compute the model-based policy gradient and compare it to the true gradient. The results are summarized in Fig. 2, where the background's opacity depicts the gradient error's magnitude and its color indicates if the respective signs of the gradients are the same (blue, ≥ 0) or differ (red, < 0). For policy optimization, the sign of the gradient estimate is paramount. However, we see in the left image that even small model errors can lead to the wrong sign of the gradient. OPC significantly reduces the magnitude of the gradient error and increases the robustness towards model errors. The definition of the signed gradient error and a more in-depth analysis of this example are presented in Appendix B.

4.2 Evaluation on Continuous Control Tasks

In the following section, we investigate the impact of OPC on a range of continuous control tasks and compare it to the current state-of-the-art model-based and model-free RL algorithms MBPO (Janner et al., 2019) and SAC (Haarnoja et al., 2018). Further, we aim to answer the important question about how data diversity affects MBRL, and OPC in particular. Having a model that can generate (theoretically) infinite amount of data is intriguing. Clearly, the benefit of having more data is limited by its quality in terms of being representative of the true environment. For OPC, the following questions arise from this consideration: Do longer rollouts help to generate more diverse data? And is there a limit on the value of simulated transition data, i.e., is more always better?

For the dynamics model $\tilde{p}^{\text{model}}$, we follow Chua et al. (2018); Janner et al. (2019) and use a probabilistic ensemble of neural networks, where each head predicts a Gaussian distribution over the next state and reward. For policy optimization, we employ SAC (Haarnoja et al., 2018). All learning curves are presented in terms of the median (lines) and interquartile range (shaded region) across 10 independent experiments, where we smooth the evaluation return with a moving average

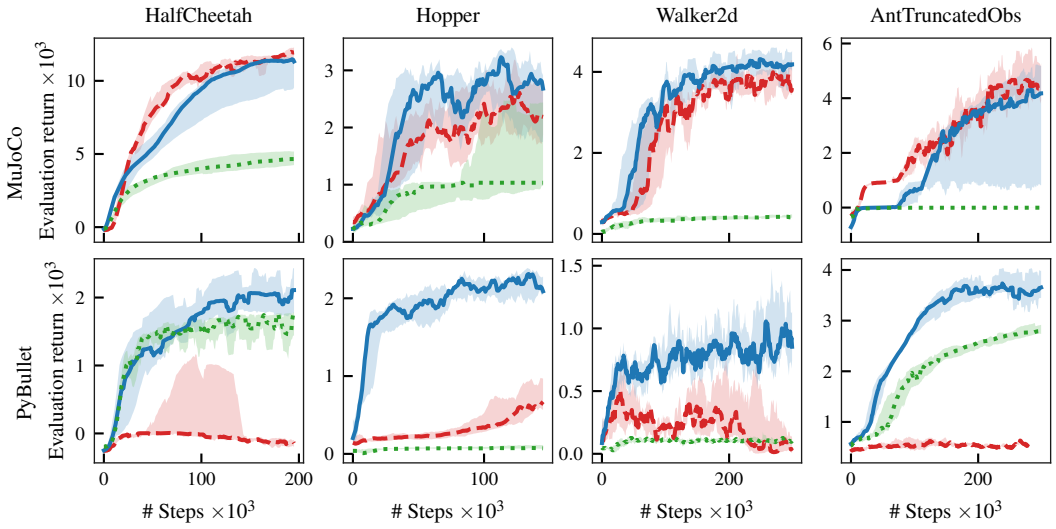

Figure 3: Comparison of OPC (), MBPO(⋆) () and SAC () on four environments from the MuJoCo control suite (top row) and their respective PyBullet implementations (bottom row). While the respective performances are comparable for the MuJoCo environments, MBPO is not able to learn successful policies for the PyBullet environments without OPC.

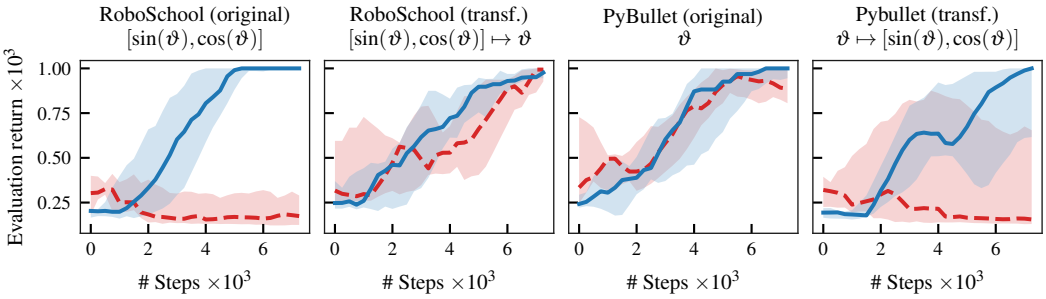

Figure 4: Comparison of OPC () and MBPO(⋆) () on different variants of the CartPole environment. When the pole's angle ϑ is observed directly (center plots), both algorithms successfully learn a policy in few episodes. When the angle is observed via sine and cosine transformations (outer two plots), MBPO(⋆) fails to solve the task.

filter to accentuate the results of particularly noisy environments. Apart from small variations in the hyperparameters, the only difference between OPC and MBPO is that our method uses $\tilde{p}^{\text{opc}}$, while MBPO uses $\tilde{p}^{\text{model}}$. Generally, we found that OPC is more robust to the choice of hyperparameters. The rollout horizon to generate training data is set to $H = 10$ for all experiments. An overview of all relevant hyperparameters is provided in Appendix E.

Our implementation is based upon the code from Janner et al. (2019). We made the following changes to the original implementation: 1) The policy is only updated at the end of an epoch, not during rollouts on the true environment. 2) The replay buffer retains data for a fixed number of episodes, to clearly distinguish on- and off-policy data. 3) For policy optimization, a small percentage of the transition tuples were not generated by the dynamics model but came directly from the true environment's transitions. We found that this design choice did not consistently improve performance and adds an additional level of complexity. Therefore, we refrain from mixing environment and model transitions and only use simulated data for policy optimization. With these minor changes, we still stay true to the key idea of MBPO and to avoid ambiguity, we denote our variant as MBPO(⋆). A more detailed comparison to the original MBPO algorithm is provided in Appendix C.3.

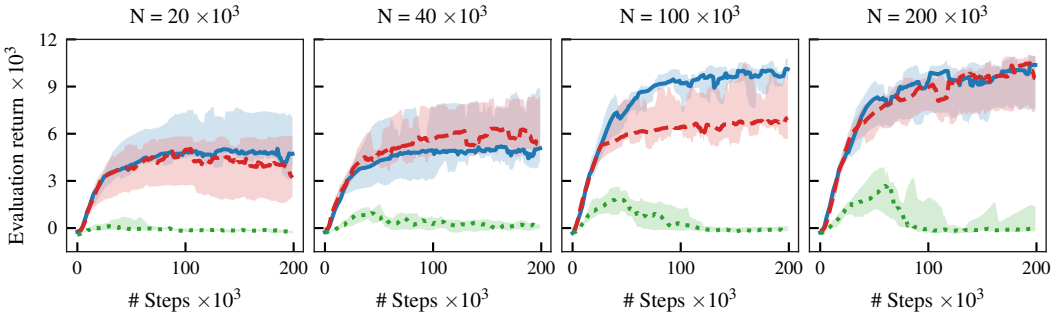

Figure 5: Ablation study for OPC on the HalfCheetah environment. In each plot, we fix the number of simulated transitions N and vary the rollout lengths $H = \{1, 5, 10\}$. The results indicate that multi-step rollouts generate more diverse data, which is required for efficient learning.

Comparative Evaluation We begin our analysis with a comparison of our method to MBPO($\star$) and SAC on four continuous control benchmark tasks from the MuJoCo control suite (Todorov et al., 2012) as well as their respective PyBullet variants (Ellenberger, 2018–2019). The results are presented in Fig. 3. We see that the difference in performance between both methods is only marginal when evaluated on the MuJoCo environments (Fig. 3, top row). Notably, the situation changes drastically for the PyBullet environments (Fig. 3, bottom row). Here, MBPO($\star$) exhibits little to no learning progress, whereas OPC succeeds at learning a good policy with few interactions in the environment. One of the main differences between the environments (apart from the physics engine itself) is that the PyBullet variants have initial state distributions with significantly larger variance.

Influence of State Representation In general, the success of RL algorithms should be agnostic to the way an environment's state is represented. In robotic applications, joint angles ϑ are oftentimes re-parameterized by a sine/cosine transformation, $\vartheta \mapsto [\sin(\vartheta), \cos(\vartheta)]$. We show that even for the simple CartPole environment, the parameterization of the pole's angle can have a large influence on the performance of an algorithm. In particular, we compare OPC and MBPO($\star$) on the RoboSchool and PyBullet variants of the CartPole environment, which represent the pole's angle with and without the sine/cosine transformation. The results are shown in Fig. 4. To rule out other effects than the angle's representation, we repeat the experiment for each implementation but transform the state to the other representation, respectively. Notably, OPC successfully learns a policy irrespective of the state's representation and the implementation, whereas MBPO($\star$) fails if the angle of the pole is represented by the sine/cosine transformation.

Influence of Data Diversity In the last experiment, we investigate if multi-step predictions are in fact beneficial compared to single-step predictions during the data generation process. To this end, we keep the total number of simulated transitions N for training constant, but choose different horizon lengths $H = \{1, 5, 10\}$. The corresponding numbers of simulated rollouts are then given by $n_{\text{rollout}} = N/H$. The results for $N = \{20, 40, 100, 200\} \times 10^3$ on the HalfCheetah environment are shown in Fig. 5. First, note that more data leads to higher asymptotic return, but after a certain point more data only leads to diminishing returns. Further, the results indicate that one-step predictions are not enough to generate sufficiently diverse data, but instead multi-step rollouts are in fact required.

5 Conclusion

In this paper, we have introduced *on-policy corrections* (OPC), a novel method to combine observed transition data with model-based predictions to mitigate model-bias in MBRL. In particular, we extend a replay buffer with a learned model to account for state-action pairs that have not been observed on the real environment. This approach enables the generation of more realistic transition data to closer match the true state distribution, which was further motivated theoretically by a tightened improvement bound on the expected return. Empirically, we demonstrated superior performance on high-dimensional continuous control tasks as well as robustness towards state representations.

REFERENCES

Pieter Abbeel, Morgan Quigley, and Andrew Y Ng. Using inaccurate models in reinforcement learning. In *International Conference on Machine Learning (ICML)*, pp. 1–8, 2006.

C.G. Atkeson and J.C. Santamaria. A comparison of direct and model-based reinforcement learning. In *Proceedings of International Conference on Robotics and Automation*, volume 4, pp. 3557–3564, 1997.

K. Baumgärtner and M. Diehl. Zero-order optimization-based iterative learning control. In *2020 59th IEEE Conference on Decision and Control (CDC)*, pp. 3751–3757, 2020. doi: 10.1109/CDC42340.2020.9303854.

Joseph K Blitzstein and Jessica Hwang. *Introduction to probability*. Crc Press, 2019.

D. A. Bristow, M. Tharayil, and A. G. Alleyne. A survey of iterative learning control. *IEEE Control Systems Magazine*, 26(3):96–114, 2006.

Jacob Buckman, Danijar Hafner, George Tucker, Eugene Brevdo, and Honglak Lee. Sample-efficient reinforcement learning with stochastic ensemble value expansion. *arXiv preprint arXiv:1807.01675*, 2018.

Frank M. Callier and Charles A. Desoer. *Linear System Theory*. Springer, New York, NY, 1991.

Yevgen Chebotar, Karol Hausman, Marvin Zhang, Gaurav Sukhatme, Stefan Schaal, and Sergey Levine. Combining model-based and model-free updates for trajectory-centric reinforcement learning. In Doina Precup and Yee Whye Teh (eds.), *Proceedings of the 34th International Conference on Machine Learning*, volume 70 of *Proceedings of Machine Learning Research*, pp. 703–711. PMLR, 06–11 Aug 2017.

Ching-An Cheng, Xinyan Yan, Nathan Ratliff, and Byron Boots. Predictor-corrector policy optimization. In *International Conference on Machine Learning*, pp. 1151–1161. PMLR, 2019.

Kurtland Chua, Roberto Calandra, Rowan McAllister, and Sergey Levine. Deep reinforcement learning in a handful of trials using probabilistic dynamics models. In S. Bengio, H. Wallach, H. Larochelle, K. Grauman, N. Cesa-Bianchi, and R. Garnett (eds.), *Advances in Neural Information Processing Systems*, volume 31. Curran Associates, Inc., 2018. URL https://proceedings.neurips.cc/paper/2018/file/3de568f8597b94bda53149c7d7f5958c-Paper.pdf.

Ignasi Clavera, Yao Fu, and Pieter Abbeel. Model-augmented actor-critic: Backpropagating through paths. In *International Conference on Learning Representations*, 2020.

Sebastian Curi, Felix Berkenkamp, and Andreas Krause. Efficient model-based reinforcement learning through optimistic policy search and planning. In H. Larochelle, M. Ranzato, R. Hadsell, M. F. Balcan, and H. Lin (eds.), *Advances in Neural Information Processing Systems*, volume 33, pp. 14156–14170. Curran Associates, Inc., 2020. URL https://proceedings.neurips.cc/paper/2020/file/a36b598abb934e4528412e5a2127b931-Paper.pdf.

Marc Deisenroth and Carl Rasmussen. Pilco: A model-based and data-efficient approach to policy search. In Lise Getoor and Tobias Scheffer (eds.), *Proceedings of the 28th International Conference on Machine Learning (ICML)*, pp. 465–472, New York, NY, USA, June 2011. ACM. ISBN 978-1-4503-0619-5.

Benjamin Ellenberger. Pybullet gymperium. https://github.com/benelot/pybullet-gym, 2018–2019.

Vladimir Feinberg, Alvin Wan, Ion Stoica, Michael I Jordan, Joseph E Gonzalez, and Sergey Levine. Model-based value estimation for efficient model-free reinforcement learning. *arXiv preprint arXiv:1803.00101*, 2018.

Tuomas Haarnoja, Aurick Zhou, Pieter Abbeel, and Sergey Levine. Soft actor-critic: Off-policy maximum entropy deep reinforcement learning with a stochastic actor. In *International Conference on Machine Learning*, pp. 1861–1870, 2018.

Michael Janner, Justin Fu, Marvin Zhang, and Sergey Levine. When to trust your model: Model-based policy optimization, 2019.

Lukasz Kaiser, Mohammad Babaeizadeh, Piotr Milos, Blazej Osinski, Roy H Campbell, Konrad Czechowski, Dumitru Erhan, Chelsea Finn, Piotr Kozakowski, Sergey Levine, et al. Model-based reinforcement learning for atari. *arXiv preprint arXiv:1903.00374*, 2019.

Sham Kakade and John Langford. Approximately optimal approximate reinforcement learning. In *Proceedings of the 19th International Conference on Machine Learning*, pp. 267–274, 2002.

Dmitry Kalashnikov, Alex Irpan, Peter Pastor, Julian Ibarz, Alexander Herzog, Eric Jang, Deirdre Quillen, Ethan Holly, Mrinal Kalakrishnan, Vincent Vanhoucke, et al. Qt-opt: Scalable deep reinforcement learning for vision-based robotic manipulation. *arXiv preprint arXiv:1806.10293*, 2018.

Gabriel Kalweit and Joschka Boedecker. Uncertainty-driven imagination for continuous deep reinforcement learning. In *Proceedings of the 1st Annual Conference on Robot Learning*, volume 78, pp. 195–206, 2017.

Diederik P. Kingma and Jimmy Ba. Adam: A method for stochastic optimization. In *International Conference on Learning Representations, ICLR*, 2015.

Daniel Kuhn, Peyman Mohajerin Esfahani, Viet Anh Nguyen, and Soroosh Shafieezadeh-Abadeh. Wasserstein distributionally robust optimization: Theory and applications in machine learning. In *Operations Research & Management Science in the Age of Analytics*, pp. 130–166. INFORMS, 2019.

Thanard Kurutach, Ignasi Clavera, Yan Duan, Aviv Tamar, and Pieter Abbeel. Model-ensemble trust-region policy optimization. *arXiv preprint arXiv:1802.10592*, 2018.

Sergey Levine and Vladlen Koltun. Guided policy search. In *International conference on machine learning*, pp. 1–9. PMLR, 2013.

Yuping Luo, Huazhe Xu, Yuanzhi Li, Yuandong Tian, Trevor Darrell, and Tengyu Ma. Algorithmic framework for model-based deep reinforcement learning with theoretical guarantees. *arXiv preprint arXiv:1807.03858*, 2018.

Ester Mariucci, Markus Reiß, et al. Wasserstein and total variation distance between marginals of lévy processes. *Electronic Journal of Statistics*, 12(2):2482–2514, 2018.

Sandipan Mishra, Ufuk Topcu, and Masayoshi Tomizuka. Optimization-based constrained iterative learning control. *IEEE Transactions on Control Systems Technology*, 19(6):1613–1621, 2010.

Volodymyr Mnih, Koray Kavukcuoglu, David Silver, Andrei A Rusu, Joel Veness, Marc G Bellemare, Alex Graves, Martin Riedmiller, Andreas K Fidjeland, Georg Ostrovski, et al. Human-level control through deep reinforcement learning. *nature*, 518(7540):529–533, 2015.

Thomas M Moerland, Joost Broekens, and Catholijn M Jonker. Model-based reinforcement learning: A survey. *arXiv preprint arXiv:2006.16712*, 2020.

David H Owens and Jari Hätönen. Iterative learning control—an optimization paradigm. *Annual reviews in control*, 29(1):57–70, 2005.

Victor M Panaretos and Yoav Zemel. Statistical aspects of wasserstein distances. *Annual review of statistics and its application*, 6:405–431, 2019.

Sébastien Racanière, Théophane Weber, David P Reichert, Lars Buesing, Arthur Guez, Danilo Rezende, Adria Puigdomenech Badia, Oriol Vinyals, Nicolas Heess, Yujia Li, et al. Imagination-augmented agents for deep reinforcement learning. In *Proceedings of the 31st International Conference on Neural Information Processing Systems*, pp. 5694–5705, 2017.

R Tyrrell Rockafellar. Integral functionals, normal integrands and measurable selections. In *Nonlinear operators and the calculus of variations*, pp. 157–207. Springer, 1976.

Stéphane Ross and Drew Bagnell. Efficient reductions for imitation learning. In *Proceedings of the thirteenth international conference on artificial intelligence and statistics*, pp. 661–668. JMLR Workshop and Conference Proceedings, 2010.

Jeff G Schneider. Exploiting model uncertainty estimates for safe dynamic control learning. *Advances in neural information processing systems*, pp. 1047–1053, 1997.

Angela Schöllig and Raffaello D'Andrea. Optimization-based iterative learning control for trajectory tracking. In *2009 European Control Conference (ECC)*, pp. 1505–1510. IEEE, 2009.

John Schulman, Sergey Levine, Pieter Abbeel, Michael Jordan, and Philipp Moritz. Trust region policy optimization. In *International conference on machine learning*, pp. 1889–1897. PMLR, 2015.

John Schulman, Filip Wolski, Prafulla Dhariwal, Alec Radford, and Oleg Klimov. Proximal policy optimization algorithms. *arXiv preprint arXiv:1707.06347*, 2017.

David Silver, Aja Huang, Chris J Maddison, Arthur Guez, Laurent Sifre, George Van Den Driessche, Julian Schrittwieser, Ioannis Antonoglou, Veda Panneershelvam, Marc Lanctot, et al. Mastering the game of go with deep neural networks and tree search. *Nature*, 529(7587):484–489, 2016.

Richard S Sutton. Integrated architectures for learning, planning, and reacting based on approximating dynamic programming. In *Machine learning proceedings 1990*, pp. 216–224. Elsevier, 1990.

Erik Talvitie. Self-correcting models for model-based reinforcement learning. In *Thirty-First AAAI Conference on Artificial Intelligence*, 2017.

Emanuel Todorov, Tom Erez, and Yuval Tassa. Mujoco: A physics engine for model-based control. In *2012 IEEE/RSJ International Conference on Intelligent Robots and Systems*, pp. 5026–5033. IEEE, 2012.

Oriol Vinyals, Igor Babuschkin, Wojciech M Czarnecki, Michaël Mathieu, Andrew Dudzik, Junyoung Chung, David H Choi, Richard Powell, Timo Ewalds, Petko Georgiev, et al. Grandmaster level in starcraft ii using multi-agent reinforcement learning. *Nature*, 575(7782):350–354, 2019.

Tianhe Yu, Garrett Thomas, Lantao Yu, Stefano Ermon, James Zou, Sergey Levine, Chelsea Finn, and Tengyu Ma. Mopo: Model-based offline policy optimization. *arXiv preprint arXiv:2005.13239*, 2020.

Baohe Zhang, Raghu Rajan, Luis Pineda, Nathan Lambert, André Biedenkapp, Kurtland Chua, Frank Hutter, and Roberto Calandra. On the importance of hyperparameter optimization for model-based reinforcement learning. In *Proceedings of The 24th International Conference on Artificial Intelligence and Statistics*, volume 130, pp. 4015–4023, 2021.

Yueqing Zhang, Bing Chu, and Zhan Shu. A preliminary study on the relationship between iterative learning control and reinforcement learning. *IFAC-PapersOnLine*, 52(29):314–319, 2019.

Barret Zoph and Quoc V Le. Neural architecture search with reinforcement learning. *arXiv preprint arXiv:1611.01578*, 2016.

A Theoretical Analysis of On-Policy Corrections

In this section, we analyze OPC from a theoretical perspective and how it affects policy improvement.

A.1 General Policy Improvement Bound

We begin by deriving inequality Eq. (5), which serves as motivation for OPC and is the foundation for the theoretical analysis. Our goal is to bound the difference in expected return for the policies before and after the policy optimization step, i.e., $\eta_{n+1} - \eta_n$. Since we are considering the MBRL setting, it is natural to express the improvement bound in terms of the expected return under the model Eq. (2) and thus obtain the following

$$\begin{aligned}
\eta_{n+1} - \eta_n &= \eta_{n+1} - \eta_n + \tilde{\eta}_{n+1} - \tilde{\eta}_{n+1} + \tilde{\eta}_n - \tilde{\eta}_n \\
&= \tilde{\eta}_{n+1} - \tilde{\eta}_n + \eta_{n+1} - \tilde{\eta}_{n+1} + \tilde{\eta}_n - \eta_n \\
\underbrace{\eta_{n+1} - \eta_n}_{\substack{\text{True policy}\\ \text{improvement}}} &\geq \underbrace{\tilde{\eta}_{n+1} - \tilde{\eta}_n}_{\substack{\text{Model policy}\\ \text{improvement}}} - \underbrace{\left|\eta_{n+1} - \tilde{\eta}_{n+1}\right|}_{\substack{\text{Off-policy}\\ \text{model error}}} - \underbrace{\left|\tilde{\eta}_n - \eta_n\right|}_{\substack{\text{On-policy}\\ \text{model error}}}.
\end{aligned}$$

According to this bound, the improvement of the policy under the true environment is governed by the three terms on the LHS:

- *Model policy improvement*: This term is what we are directly optimizing in MBRL Eq. (2) offset by the return of the previous iteration $\tilde{\eta}_n$, which is constant given the current policy π_n. Assuming that we are not at an optimum, standard policy optimization algorithms guarantee that this term is non-negative.
- *Off-policy model error*: The last term is the difference in return for the true environment and model under the improved policy π_{n+1}. This depends largely on the generalization properties of our model, since it is not trained on data under π_{n+1}.
- *On-policy model error*: This term compares the on-policy return under π_n between the true environment and the model and it is zero for any model $\tilde{p} = p$. Since we have access to transitions from the true environment under the π_n, the replay buffer Eq. (3) fulfills this condition under certain circumstances and the on-policy model error vanishes, see Lemma 2.

Note that the learned model Eq. (4) is able to generalize to unseen state-action pairs better than the replay buffer Eq. (3) and accordingly will achieve a lower off-policy model error. The motivation behind OPC is therefore to combine the best of the learned model and the replay buffer to reduce both on- and off-policy model errors.

A.2 Properties of the Replay Buffer

The benefit of the replay buffer Eq. (3) is that it can never introduce any model-bias such that any trajectory sampled from this model is guaranteed to come from the true state distribution. Accordingly, if we have collected sufficient data under the same policy, the on-policy model error vanishes.

Lemma 2. *Let M be the true MDP with (stochastic) dynamics p, bounded reward $r < r_{\max}$ and let $\tilde{p}^{\text{replay}}$ be the transition model for the replay buffer Eq. (3). Further, consider a set of trajectories $\mathcal{D} = \bigcup_{b=1}^{B} \{(\hat{\mathbf{s}}_t^b, \hat{\mathbf{a}}_t^b, \hat{\mathbf{s}}_{t+1}^b)\}_{t=0}^{T-1}$ collected from M under policy π. If we collect more and more on-policy training data under the same policy, then*

$$\lim_{B\to\infty} \Pr\left(|\eta - \tilde{\eta}^{\text{replay}}| > \varepsilon\right) = 0 \quad \forall \varepsilon$$

where $\tilde{\eta}^{\text{replay}}$ is the expected return under the replay buffer using the collected trajectories $\mathcal{D}$.

Proof. First, note that the corresponding expected return for the replay-buffer model is given by

$$\tilde{\eta}^{\text{replay}} = \frac{1}{B} \sum_{b=1}^{B} \sum_{t=0}^{T-1} r(\hat{\mathbf{s}}_t^b, \hat{\mathbf{a}}_t^b),$$

which is a sample-based approximation of the true reward η. By the weak law of large numbers (see e.g., Blitzstein & Hwang (2019, Theorem 10.2.2)), the Lemma then holds. □

A.3 PROPERTIES OF THE LEARNED MODEL

Following Janner et al. (2019, Lemma B.3), a general bound on the performance gap between two MDPs with different dynamics can be given by

$$|\eta_1 - \eta_2| \leq 2 r_{\max} \epsilon_m \sum_{t=1}^{H} t\gamma^t. \tag{11}$$

where $\epsilon_m \geq \max_t \mathbb{E}_{\mathbf{s}\sim p_1^t(\mathbf{s})} \mathrm{KL}(p_1(\mathbf{s}', \mathbf{a}) || p_2(\mathbf{s}', \mathbf{a}))$ bounds the mismatch between the respective transition models. Now, the final form of Eq. (11) depends on the horizon length H. For $H \to \infty$, we obtain the original result form Janner et al. (2019) with $\sum_{t\geq 1} t\gamma^t = \gamma/(1-\gamma)^2$. For the finite horizon case and H being smaller than the effective horizon encoded in the discount factor $H < \gamma/(1-\gamma)$, the following bound holds:

$$\sum_{t=1}^{H} t\gamma^t \leq \min\Big\{\frac{H(H-1)}{2}, \frac{H}{1-\gamma}\Big\}, \tag{12}$$

which can be easily verified by upper bounding $t \leq H$ to obtain $H/(1-\gamma)$ or by bounding $\gamma \leq 1$ to obtain $\mathcal{O}(H^2)$.

A.4 PROPERTIES OF OPC

In this section, we analyze the properties of OPC relative to the true, unknown environment's transition distribution p and a learned representation $\tilde{p}$. In general, the OPC-model mixes observed transitions from the environment with the learned model. The resulting transitions are then a combination of the mean transitions from the learned model, the aleatoric noise from the data (the environment), and the mean-error between our learned model and the environment.

A.4.1 PROOF OF LEMMA 1

In this section we proof Lemma 1 by showing that the OPC-model coincides with the replay-buffer Eq. (3) in the case of a deterministic policy and thus lead to the same expected return $\tilde{\eta}$.

Lemma 3. *Let M be the true MDP with (stochastic) dynamics p and let $\tilde{M}$ be a MDP with the same reward function r and initial state distribution ρ_0, but different dynamics $\tilde{p}^{\text{model}}$, respectively. Further, assume a deterministic policy $\pi : \mathcal{S} \mapsto \mathcal{A}$ and a set of trajectories $\mathcal{D} = \bigcup_{b=1}^{B} \{(\hat{\mathbf{s}}_t^b, \hat{\mathbf{a}}_t^b, \hat{\mathbf{s}}_{t+1}^b)\}_{t=0}^{T-1}$ collected from M under π. If we extend the approximate dynamics $\tilde{p}^{\text{model}}$ by* OPC *with data $\mathcal{D}$, then*

$$\tilde{\eta}^{\text{replay}} = \eta^{\text{opc}},$$

where $\tilde{\eta}^{\text{replay}}$ and $\tilde{\eta}^{\text{opc}}$ are the model-based returns following models Eqs. (3) *and* (6)*, respectively.*

Proof. For the proof, it suffices to show that the resulting state distributions of the two transition models $\tilde{p}^{\text{replay}}$ and $\tilde{p}^{\text{opc}}$ under the deterministic policy π are the same for all b with $1 \leq b \leq B$. We show this by induction:

For $t = 0$ the states are sampled from the initial state distribution, thus we have $\mathbf{s}_0 = \hat{\mathbf{s}}_0^b$ by definition. Assume that $\mathbf{s}_t = \hat{\mathbf{s}}_t^b$ as an induction hypothesis. Then

$$\begin{aligned}
\tilde{p}^{\text{opc}}(\mathbf{s}_{t+1} \mid \mathbf{s}_t, \pi(\mathbf{s}_t), b) &= \delta\Big(\mathbf{s}_{t+1} - \hat{\mathbf{s}}_{t+1}^b\Big) * \delta\Big(\mathbf{s}_{t+1} - \Big[f(\mathbf{s}_t, \pi(\mathbf{s}_t)) - f(\hat{\mathbf{s}}_t^b, \hat{\mathbf{a}}_t^b)\Big]\Big) \\
&= \delta\Big(\mathbf{s}_{t+1} - \Big[\hat{\mathbf{s}}_{t+1}^b + f(\mathbf{s}_t, \pi(\mathbf{s}_t)) - f(\hat{\mathbf{s}}_t^b, \hat{\mathbf{a}}_t^b)\Big]\Big) \\
&= \delta\Big(\mathbf{s}_{t+1} - \Big[\hat{\mathbf{s}}_{t+1}^b + f(\hat{\mathbf{s}}_t^b, \hat{\mathbf{a}}_t^b) - f(\hat{\mathbf{s}}_t^b, \hat{\mathbf{a}}_t^b)\Big]\Big) \\
&= \delta\Big(\mathbf{s}_{t+1} - \hat{\mathbf{s}}_{t+1}^b\Big) \\
&= \tilde{p}^{\text{replay}}(\mathbf{s}_{t+1} \mid t+1, b)
\end{aligned}$$

where the second step follows by the induction hypothesis and due to the deterministic policy. Thus, for any index b we have $\tau_b^{\text{opc}} = \tau_b$ and the result follows. □

Now, combining Lemmas 2 and 3 proofs the result in Lemma 1.

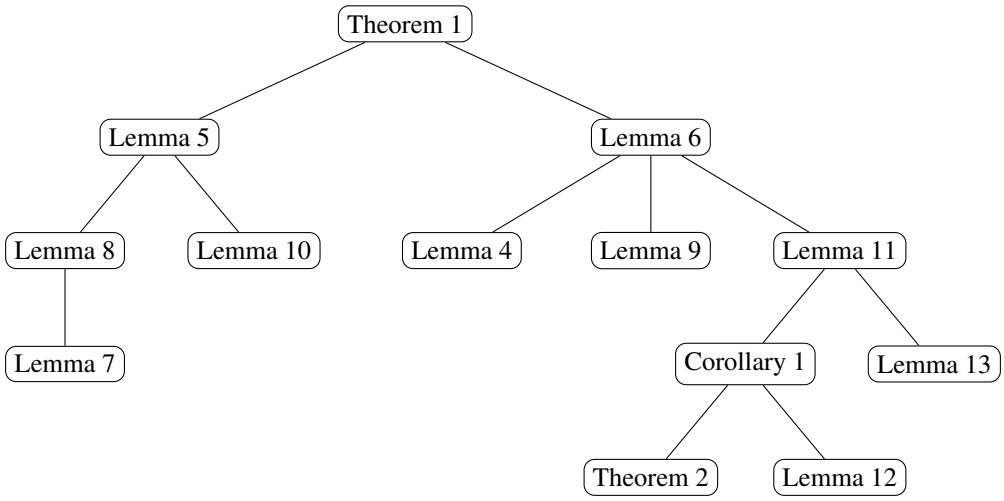

Figure 6: Overview about the supporting Lemmas for the proof of Theorem 1.

A.4.2 Proof of Theorem 1

Remark on Notation In the main paper, we unify the notation for state sequence probabilities of the different models Eqs. (3), (4) and (6) as $\tilde{p}^{\mathrm{x}}(\tau_{t:t+H} \mid t, b)$ with $\mathrm{x} \in \{\text{replay}, \text{model}, \text{opc}\}$. This allows for a consistent description of the respective rollouts independent of the model being a learned representation, a replay buffer or the OPC-model. For that notation, the index b denotes the sampled trajectory from the collected data on the real environment. Implicitly, we therefore condition the state sequence probability on the observed transition tuples $[(\hat{\mathbf{s}}^b_{t+1}, \hat{\mathbf{s}}^b_t, \hat{\mathbf{a}}^b_t), \ldots, (\hat{\mathbf{s}}^b_{t+H}, \hat{\mathbf{s}}^b_{t+H-1}, \hat{\mathbf{a}}^b_{t+H-1})]$, i.e.,

$$\tilde{p}^{\mathrm{x}}(\tau_{t:t+H} \mid t, b) = \tilde{p}^{\mathrm{x}}(\tau_{t:t+H} \mid (\hat{\mathbf{s}}^b_{t+1}, \hat{\mathbf{s}}^b_t, \hat{\mathbf{a}}^b_t), \ldots, (\hat{\mathbf{s}}^b_{t+H}, \hat{\mathbf{s}}^b_{t+H-1}, \hat{\mathbf{a}}^b_{t+H-1})), \tag{13}$$

where we omit the explicit conditioning for the sake of brevity in the main paper. Similarly, we can write the one-step model Eq. (6) for OPC in an explicit form as

$$\tilde{p}^{\mathrm{opc}}(\mathbf{s}_{t+1}|\mathbf{s}_t, \mathbf{a}_t, b) = \tilde{p}^{\mathrm{opc}}(\mathbf{s}_{t+1}|\mathbf{s}_t, \mathbf{a}_t, \hat{\mathbf{s}}^b_{t+1}, \hat{\mathbf{s}}^b_t, \hat{\mathbf{a}}^b_t). \tag{14}$$

Note that with the explicit notation, the relation between the OPC-model Eq. (6) and *generalized* OPC-model Eq. (7) becomes clear:

$$\tilde{p}^{\mathrm{opc}}_{\star}(\mathbf{s}_{t+1} \mid \mathbf{s}_t, \mathbf{a}_t, b) = \tilde{p}^{\mathrm{opc}}(\mathbf{s}_{t+1} \mid \mathbf{s}_t, \mathbf{a}_t, \hat{\mathbf{s}}^b_t, \hat{\mathbf{a}}^b_t) = \int \tilde{p}^{\mathrm{opc}}(\mathbf{s}_{t+1} \mid \mathbf{s}_t, \mathbf{a}_t, \hat{\mathbf{s}}^b_{t+1} \hat{\mathbf{s}}^b_t, \hat{\mathbf{a}}^b_t) \, \mathrm{d}\hat{\mathbf{s}}^b_{t+1}. \tag{15}$$

For the following proofs, we will stay with the explicit notation for sake of clarity and instead omit the conditioning on b.

Generalized OPC-Model In this section, we have a closer look at the *generalized* OPC-model Eq. (7). The main difference between Eqs. (6) and (7) is that the former is in fact transitioning deterministically (the stochasticity arises from the environment's aleatoric uncertainty which manifests itself in the observed transitions). The two models can be related via marginalization of $\hat{\mathbf{s}}^b_{t+1}$, see Eq. (15). The resulting generalized OPC-model can then be related to the true transition distribution according to the following Lemma.

Lemma 4. *For all $\hat{\mathbf{s}}^b_t, \hat{\mathbf{a}}^b_t \in \mathcal{S} \times \mathcal{A}$ with $\hat{\mathbf{s}}^b_{t+1} \sim p(\hat{\mathbf{s}}_{t+1} \mid \hat{\mathbf{s}}^b_t, \hat{\mathbf{a}}^b_t)$ it holds that*

$$\tilde{p}^{\mathrm{opc}}(\mathbf{s}_{t+1} \mid \mathbf{s}_t, \mathbf{a}_t, \hat{\mathbf{s}}^b_t, \hat{\mathbf{a}}^b_t) = p\Big(\mathbf{s}_{t+1} - \underbrace{\big[\tilde{f}(\mathbf{s}_t, \mathbf{a}_t) - \tilde{f}(\hat{\mathbf{s}}^b_t, \hat{\mathbf{a}}^b_t)\big]}_{\text{Mean correction}} \mid \mathbf{s}_t, \mathbf{a}_t, \hat{\mathbf{s}}^b_t, \hat{\mathbf{a}}^b_t\Big), \tag{16}$$

where $\tilde{f}(\mathbf{s}_t, \mathbf{a}_t) = \mathbb{E}[\tilde{p}^{\mathrm{model}}(\mathbf{s}_{t+1} \mid \mathbf{s}_t, \mathbf{a}_t)]$ is the mean transition of the learned model Eq. (4) *and $\tilde{p}^{\mathrm{opc}}(\mathbf{s}_{t+1} \mid \mathbf{s}_t, \mathbf{a}_t, \hat{\mathbf{s}}^b_t, \hat{\mathbf{a}}^b_t)$ denotes the* OPC*-model if we marginalize over the distribution for $\hat{\mathbf{s}}^b_{t+1}$ instead of using its observed value.*

Proof. Using the explicit notation Eq. (14), the OPC-model from Eq. (6) is defined as

$$\tilde{p}^{\text{opc}}(\mathbf{s}_{t+1} \mid \mathbf{s}_t, \mathbf{a}_t, b) = \tilde{p}^{\text{opc}}(\mathbf{s}_{t+1} \mid \mathbf{s}_t, \mathbf{a}_t, \hat{\mathbf{s}}_t^b, \hat{\mathbf{a}}_t^b, \hat{\mathbf{s}}_{t+1}^b) \tag{17}$$

$$= \delta\Big(\mathbf{s}_{t+1} - \hat{\mathbf{s}}_{t+1}^b\Big) * \delta\Big(\mathbf{s}_{t+1} - \Big[\tilde{f}(\mathbf{s}_t, \mathbf{a}_t) - \tilde{f}(\hat{\mathbf{s}}_t^b, \hat{\mathbf{a}}_t^b)\Big]\Big), \tag{18}$$

$$= \delta\Big(\mathbf{s}_{t+1} - \Big[\hat{\mathbf{s}}_{t+1}^b + \tilde{f}(\mathbf{s}_t, \mathbf{a}_t) - \tilde{f}(\hat{\mathbf{s}}_t^b, \hat{\mathbf{a}}_t^b)\Big]\Big). \tag{19}$$

With $\hat{\mathbf{s}}_{t+1}^b \sim p(\hat{\mathbf{s}}_{t+1} \mid \hat{\mathbf{s}}_t^b, \hat{\mathbf{a}}_t^b)$, marginalizing $\hat{\mathbf{s}}_{t+1}$ yields (note that we use $\hat{\mathbf{s}}_{t+1}$ instead of $\mathbf{s}_{t+1}$ to denote the random variable for the next state in order to distinguish it from the random variable for $\tilde{p}^{\text{opc}}(\mathbf{s}_{t+1} \mid \mathbf{s}_t, \mathbf{a}_t, b)$ under the integral)

$$\tilde{p}^{\text{opc}}(\mathbf{s}_{t+1} \mid \mathbf{s}_t, \mathbf{a}_t, \hat{\mathbf{s}}_t^b, \hat{\mathbf{a}}_t^b) = \int \delta\Big(\mathbf{s}_{t+1} - \Big[\hat{\mathbf{s}}_{t+1} + \tilde{f}(\mathbf{s}_t, \mathbf{a}_t) - \tilde{f}(\hat{\mathbf{s}}_t^b, \hat{\mathbf{a}}_t^b)\Big]\Big) p(\hat{\mathbf{s}}_{t+1} \mid \hat{\mathbf{s}}_t^b, \hat{\mathbf{a}}_t^b)\, \mathrm{d}\hat{\mathbf{s}}_{t+1},$$

$$= p\Big(\mathbf{s}_{t+1} - \big[\tilde{f}(\mathbf{s}_t, \mathbf{a}_t) - \tilde{f}(\hat{\mathbf{s}}_t^b, \hat{\mathbf{a}}_t^b)\big] \mid \hat{\mathbf{s}}_t^b, \hat{\mathbf{a}}_t^b\Big).$$

□

Remark 1. An alternative way of writing the general OPC-model is the following,

$$\tilde{p}^{\text{opc}}(\mathbf{s}_{t+1} \mid \mathbf{s}_t, \mathbf{a}_t, \hat{\mathbf{s}}_t^b, \hat{\mathbf{a}}_t^b) = \underbrace{p(\hat{\mathbf{s}}_{t+1} \mid \hat{\mathbf{s}}_t^b, \hat{\mathbf{a}}_t^b)}_{\text{On-policy transition}} * \underbrace{\delta\Big(\mathbf{s}_{t+1} - \Big[\tilde{f}(\mathbf{s}_t, \mathbf{a}_t) - \tilde{f}(\hat{\mathbf{s}}_t^b, \hat{\mathbf{a}}_t^b)\Big]\Big)}_{\text{Mean correction term}}, \tag{20}$$

which highlights that the $\tilde{p}^{\text{opc}}$ transitions according to the true on-policy dynamics conditioned on data from the replay buffer, combined with a correction term. We can further explicitly see why an implementation of this model wouldn't be possible due to its dependency on the true transition probabilities. Thus, in practice, we're limited to the sample-based approximation shown in the paper.

The fundamental idea for the proof of Theorem 1 lies in the following Lemma 5, which is the foundation for bounding the on-policy error. The Wasserstein distance naturally arises in bounding this type of error model as it depends on the expected return under two different distributions. The final result is then summarized in Theorem 1.

Lemma 5. *Let $\tilde{p}^{\text{opc}}$ be the generalized* OPC*-model (cf. Lemma 4) and $\tilde{\eta}^{\text{opc}}$ be its corresponding expected return. Assume that the return $r(\mathbf{s}_t, \mathbf{a}_t)$ is L_r-Lipschitz and the policy $\pi(\mathbf{a}_t \mid \mathbf{s}_t)$ is L_π-Lipschitz with respect to $\mathbf{s}_t$ under the Wasserstein distance, then*

$$|\eta - \tilde{\eta}^{\text{opc}}| \leq L_r \sqrt{1 + L_\pi^2} \sum_{t \geq 0} \gamma^t \mathcal{W}_2(p(\mathbf{s}_t), \tilde{p}^{\text{opc}}(\mathbf{s}_t)) \tag{21}$$

Proof.

$$|\eta - \tilde{\eta}^{\text{opc}}| = \Big| \mathop{\mathbb{E}}_{\tau \sim p}\Big[\sum_{t \geq 0} \gamma^t r(\hat{\mathbf{s}}_t, \hat{\mathbf{a}}_t)\Big] - \mathop{\mathbb{E}}_{\tau \sim \tilde{p}^{\text{opc}}}\Big[\sum_{t \geq 0} \gamma^t r(\mathbf{s}_t, \mathbf{a}_t)\Big]\Big| \tag{22}$$

$$= \Big| \sum_{t \geq 0} \gamma^t \Big(\mathop{\mathbb{E}}_{\hat{\mathbf{s}}_t, \hat{\mathbf{a}}_t \sim p(\hat{\mathbf{s}}_t, \hat{\mathbf{a}}_t)} \big[r(\hat{\mathbf{s}}_t, \hat{\mathbf{a}}_t)\big] - \mathop{\mathbb{E}}_{\mathbf{s}_t, \mathbf{a}_t \sim \tilde{p}^{\text{opc}}(\mathbf{s}_t, \mathbf{a}_t)} \big[r(\mathbf{s}_t, \mathbf{a}_t)\big]\Big)\Big| \tag{23}$$

$$\leq \sum_{t \geq 0} \gamma^t \Big| \mathop{\mathbb{E}}_{\hat{\mathbf{s}}_t, \hat{\mathbf{a}}_t \sim p(\hat{\mathbf{s}}_t, \hat{\mathbf{a}}_t)} \big[r(\hat{\mathbf{s}}_t, \hat{\mathbf{a}}_t)\big] - \mathop{\mathbb{E}}_{\mathbf{s}_t, \mathbf{a}_t \sim \tilde{p}^{\text{opc}}(\mathbf{s}_t, \mathbf{a}_t)} \big[r(\mathbf{s}_t, \mathbf{a}_t)\big]\Big| \tag{24}$$

Applying Lemma 8:

$$\leq \sum_{t \geq 0} \gamma^t L_r \mathcal{W}_2(p(\hat{\mathbf{s}}_t, \hat{\mathbf{a}}_t), \tilde{p}^{\text{opc}}(\mathbf{s}_t, \mathbf{a}_t)) \tag{25}$$

Writing the joint distributions for state/action in terms of their conditional (i.e., policy) and marginal distributions $p(\mathbf{s}_t, \mathbf{a}_t) = \pi(\mathbf{a}_t \mid \mathbf{s}_t) p(\mathbf{s}_t)$:

$$= \sum_{t \geq 0} \gamma^t L_r \mathcal{W}_2(\pi(\hat{\mathbf{a}}_t \mid \hat{\mathbf{s}}_t) p(\hat{\mathbf{s}}_t), \pi(\mathbf{a}_t \mid \mathbf{s}_t) \tilde{p}^{\text{opc}}(\mathbf{s}_t)) \tag{26}$$

Under the assumption that the policies π are L_π-Lipschitz under the Wasserstein distance, application of Lemma 10 concludes the proof:

$$\leq \sum_{t\geq 0} \gamma^t L_r \sqrt{1+L_\pi^2}\mathcal{W}_2(p(\hat{\mathbf{s}}_t), \tilde{p}^{\text{opc}}(\mathbf{s}_t)). \tag{27}$$

□

Lemma 6 (Wasserstein Distance between Marginal State Distributions)**.** *Let $\tilde{p}^{\text{opc}}(\mathbf{s}_t)$ and $p(\hat{\mathbf{s}}_t)$ be the marginal state distributions at time t when rolling out from the same initial state $\hat{\mathbf{s}}_0$ under the same policy with the* OPC*-model and the true environment, respectively. Assume that the underlying learned dynamics model is L_f-Lipschitz continuous with respect to both its arguments and the policy $\pi(\mathbf{a} \mid \mathbf{s})$ is L_π-Lipschitz with respect to $\mathbf{s}$ under the Wasserstein distance. If it further holds that the policy's (co-)variance $\text{Var}[\pi(\mathbf{a} \mid \mathbf{s})] = \Sigma_\pi(\mathbf{s}) \in \mathbb{S}_+^{|\mathcal{A}|}$ is finite over the complete state space, i.e., $\max_{\mathbf{s}\in\mathcal{S}} \text{trace}\{\Sigma_\pi(\mathbf{s})\} \leq \bar{\sigma}_\pi^2$, then the discrepancy between the marginal state distributions of the two models is bounded*

$$\mathcal{W}_2^2(\tilde{p}^{\text{opc}}(\mathbf{s}_t), p(\hat{\mathbf{s}}_t)) \leq 2\sqrt{|\mathcal{A}|}\bar{\sigma}_\pi^2 L_f^2 \sum_{t'=0}^{t-1} (L_f^2 + L_\pi^2)^{t'} \tag{28}$$

Proof. We proof the Lemma by induction.

Base Case: $t = 1$ For the base case, we need to show that starting from the same initial state $\hat{\mathbf{s}}_0$ the following condition holds:

$$\mathcal{W}_2^2(\tilde{p}^{\text{opc}}(\mathbf{s}_1), p(\hat{\mathbf{s}}_1)) \leq 2\sqrt{|\mathcal{A}|}\bar{\sigma}_\pi^2 L_f^2$$

For ease of readability, we define $\mathbf{z} = (\mathbf{s}, \mathbf{a})$ and use the notation $\mathrm{d}p(\mathbf{x}, \mathbf{y}) = p(\mathbf{x}, \mathbf{y})\,\mathrm{d}\mathbf{x}\,\mathrm{d}\mathbf{y}$ whenever no explicit assumptions are made about the distributions.

$$\mathcal{W}_2(\tilde{p}^{\text{opc}}(\mathbf{s}_1), p(\hat{\mathbf{s}}_1)) \tag{29}$$

$$= \mathcal{W}_2\left(\iint \tilde{p}^{\text{opc}}(\mathbf{s}_1 \mid \hat{\mathbf{z}}_0, \mathbf{z}_0)\,\mathrm{d}p(\hat{\mathbf{z}}_0, \mathbf{z}_0), \int p(\hat{\mathbf{s}}_1 \mid \hat{\mathbf{z}}_0)\,\mathrm{d}p(\hat{\mathbf{z}}_0)\right) \tag{30}$$

Recall that we can write both $\tilde{p}^{\text{opc}}$ and p as convolution between p_ϵ and a Dirac delta (see Lemma 4). Together with the identity Eq. (55), the Wasserstein distance for sums of random variables Eq. (54) and noting $\mathcal{W}_p(p_\epsilon(\epsilon), p_\epsilon(\epsilon)) = 0$:

$$\leq \mathcal{W}_2\left(\iint \delta(\mathbf{s}_1 - [f(\hat{\mathbf{z}}_0) + \tilde{f}(\mathbf{z}_0) - \tilde{f}(\hat{\mathbf{z}}_0)])\,\mathrm{d}p(\hat{\mathbf{z}}_0, \mathbf{z}_0), \int \delta(\hat{\mathbf{s}}_1 - f(\hat{\mathbf{z}}_0))\,\mathrm{d}p(\hat{\mathbf{z}}_0)\right) \tag{31}$$

Squaring and using Lemma 9:

$$\mathcal{W}_2^2\left(\iint \delta(\mathbf{s}_1 - [f(\hat{\mathbf{z}}_0) + \tilde{f}(\mathbf{z}_0) - \tilde{f}(\hat{\mathbf{z}}_0)])\,\mathrm{d}p(\hat{\mathbf{z}}_0)p(\mathbf{z}_0), \int \delta(\hat{\mathbf{s}}_1 - f(\hat{\mathbf{z}}_0))\,\mathrm{d}p(\hat{\mathbf{z}}_0)\right)$$

$$\leq \iint \|f(\hat{\mathbf{z}}_0) + \tilde{f}(\mathbf{z}_0) - \tilde{f}(\hat{\mathbf{z}}_0) - f(\hat{\mathbf{z}}_0)\|^2\,\mathrm{d}p(\hat{\mathbf{z}}_0, \mathbf{z}_0) \tag{32}$$

$$= \iint \|\tilde{f}(\mathbf{z}_0) - \tilde{f}(\hat{\mathbf{z}}_0)\|^2\,\mathrm{d}p(\hat{\mathbf{z}}_0, \mathbf{z}_0) \tag{33}$$

$$\leq L_f^2 \int \|\mathbf{s}_0 - \hat{\mathbf{s}}_0\|^2 + \|\mathbf{a}_0 - \hat{\mathbf{a}}_0\|^2\,\mathrm{d}p(\hat{\mathbf{s}}_0, \hat{\mathbf{a}}_0, \mathbf{s}_0, \mathbf{a}_0) \tag{34}$$

We are assuming that the initial states of the trajectory rollouts coincide. The joint state/action distribution can then be written as $p(\hat{\mathbf{s}}_0, \hat{\mathbf{a}}_0, \mathbf{s}_0, \mathbf{a}_0) = p(\hat{\mathbf{s}}_0)\pi(\hat{\mathbf{a}}_0 \mid \hat{\mathbf{s}}_0)\delta(\mathbf{s}_0 - \hat{\mathbf{s}}_0)\pi(\mathbf{a}_0 \mid \mathbf{s}_0)$. Integrating with respect to $\mathbf{s}_0$ leads to:

$$= L_f^2 \int \|\mathbf{a}_0 - \hat{\mathbf{a}}_0\|^2 p(\hat{\mathbf{s}}_0)\pi(\hat{\mathbf{a}}_0 \mid \hat{\mathbf{s}}_0)\pi(\mathbf{a}_0 \mid \hat{\mathbf{s}}_0)\,\mathrm{d}\hat{\mathbf{s}}_0\,\mathrm{d}\hat{\mathbf{a}}_0\,\mathrm{d}\mathbf{a}_0 \tag{35}$$

This term describes the mean squared distance between two random actions. Since we condition π on the same state $\hat{\mathbf{s}}_0$, the policy distributions coincide. Define $\Delta\mathbf{a} = \mathbf{a}_0 - \hat{\mathbf{a}}_0$,

$$= L_f^2 \mathop{\mathbb{E}}_{\hat{\mathbf{s}}_0} \big[\mathop{\mathbb{E}}_{\Delta\mathbf{a}} [\|\Delta\mathbf{a}\|^2] \big] \tag{36}$$

$$= L_f^2 \mathop{\mathbb{E}}_{\hat{\mathbf{s}}_0} \big[\operatorname{trace}\{\operatorname{Var}[\Delta\mathbf{a}]\} \big] \tag{37}$$

Now $\operatorname{Var}[\Delta\mathbf{a}] = \operatorname{Var}[\pi(\hat{\mathbf{a}}_0 \mid \hat{\mathbf{s}}_0)] + \operatorname{Var}[\pi(\mathbf{a}_0 \mid \hat{\mathbf{s}}_0)] = 2\operatorname{Var}[\pi(\mathbf{a}_0 \mid \hat{\mathbf{s}}_0)]$

$$= 2L_f^2 \mathop{\mathbb{E}}_{\hat{\mathbf{s}}_0} \big[\operatorname{trace}\{\operatorname{Var}[\pi(\mathbf{a}_0 \mid \hat{\mathbf{s}}_0)]\} \big] \tag{38}$$

This term is in fact less than Eq. (28) for $t = 0$, thus proofing the base case.

$$\leq 2\sqrt{|\mathcal{A}|}\bar{\sigma}_\pi^2 L_f^2 \tag{39}$$

Inductive Step We will show that if the hypothesis holds for t then it holds for $t+1$ as well. We explicitly write the following intermediate bound such that its application in the proof is more apparent, i.e.,

$$\mathcal{W}_2^2(p(\hat{\mathbf{s}}_t), \tilde{p}^{\text{opc}}(\mathbf{s}_t)) \leq \int \|\tilde{f}(\mathbf{z}_{t-1}) - \tilde{f}(\hat{\mathbf{z}}_{t-1})\|^2 \,\mathrm{d}p(\hat{\mathbf{z}}_{t-1}, \mathbf{z}_{t-1}) \tag{40}$$

$$\leq 2\sqrt{|\mathcal{A}|}\bar{\sigma}_\pi^2 L_f^2 \sum_{t'=0}^{t-1} (L_f^2 + L_\pi^2)^{t'}, \tag{41}$$

where the first inequality immediately follows from the same reasoning as in the base case Eq. (29)–Eq. (33).

$$\mathcal{W}_2^2(p(\hat{\mathbf{s}}_{t+1}, p(\mathbf{s}_{t+1})) \tag{42}$$

$$\leq \int \|\tilde{f}(\mathbf{z}_t) - \tilde{f}(\hat{\mathbf{z}}_t)\|^2 \,\mathrm{d}p(\hat{\mathbf{z}}_t, \mathbf{z}_t) \tag{43}$$

$$\leq L_f^2 \int \|\mathbf{s}_t - \hat{\mathbf{s}}_t\|^2 \,\mathrm{d}p(\hat{\mathbf{z}}_t, \mathbf{z}_t) + L_f^2 \int \|\mathbf{a}_t - \hat{\mathbf{a}}_t\|^2 \,\mathrm{d}p(\hat{\mathbf{z}}_t, \mathbf{z}_t) \tag{44}$$

Applying Lemma 11 to the second integral

$$\leq (L_f^2 + L_\pi^2) \int \|\mathbf{s}_t - \hat{\mathbf{s}}_t\|^2 \,\mathrm{d}p(\hat{\mathbf{z}}_t, \mathbf{z}_t) + 2\sqrt{|\mathcal{A}|}L_f^2\bar{\sigma}_\pi^2 \tag{45}$$

We predict along a consistent trajectory, i.e., $\mathbf{s}_t = \hat{\mathbf{s}}_t + \tilde{f}(\mathbf{s}_{t-1}, \mathbf{a}_{t-1}) - \tilde{f}(\hat{\mathbf{s}}_{t-1}, \hat{\mathbf{a}}_{t-1})$

$$\leq (L_f^2 + L_\pi^2) \int \|\tilde{f}(\mathbf{z}_{t-1}) - \tilde{f}(\hat{\mathbf{z}}_{t-1})\|^2 \,\mathrm{d}p(\hat{\mathbf{z}}_{t-1}, \mathbf{z}_{t-1}) + 2\sqrt{|\mathcal{A}|}L_f^2\bar{\sigma}_\pi^2 \tag{46}$$

Assume that the hypothesis Eq. (40) holds for t

$$\leq (L_f^2 + L_\pi^2) \times 2\sqrt{|\mathcal{A}|}\bar{\sigma}_\pi^2 L_f^2 \sum_{t'=0}^{t-1} (L_f^2 + L_\pi^2)^{t'} + 2\sqrt{|\mathcal{A}|}L_f^2\bar{\sigma}_\pi^2 \tag{47}$$

$$= 2\sqrt{|\mathcal{A}|}\bar{\sigma}_\pi^2 L_f^2 \big[1 + \sum_{t'=0}^{t-1} (L_f^2 + L_\pi^2)^{t'}\big] \tag{48}$$

$$= 2\sqrt{|\mathcal{A}|}\bar{\sigma}_\pi^2 L_f^2 \sum_{t'=0}^{t} (L_f^2 + L_\pi^2)^{t'} \tag{49}$$

□

Theorem 1. *Let $\tilde{\eta}_\star^{\text{opc}}$ and η be the expected return under the generalized* OPC*-model Eq.* (7) *and the true environment, respectively. Assume that the learned model's mean transition function $\tilde{f}(\mathbf{s}_t, \mathbf{a}_t) = \mathbb{E}[\tilde{p}^{\text{model}}(\mathbf{s}_{t+1} \mid \mathbf{s}_t, \mathbf{a}_t)]$ is L_f-Lipschitz and the reward $r(\mathbf{s}_t, \mathbf{a}_t)$ is L_r-Lipschitz. Further, if the policy $\pi(\mathbf{a}_t \mid \mathbf{s}_t)$ is L_π-Lipschitz with respect to $\mathbf{s}_t$ under the Wasserstein distance and its (co-)variance $\operatorname{Var}[\pi(\mathbf{a}_t \mid \mathbf{s}_t)] = \Sigma_\pi(\mathbf{s}_t) \in \mathbb{S}_+^{|\mathcal{A}|}$ is finite over the complete state space, i.e., $\max_{\mathbf{s}_t \in \mathcal{S}} \operatorname{trace}\{\Sigma_\pi(\mathbf{s}_t)\} \leq \bar{\sigma}_\pi^2$, then with $C_1 = \sqrt{2(1 + L_\pi^2)}L_f L_r$ and $C_2 = \sqrt{L_f^2 + L_\pi^2}$*

$$|\eta - \tilde{\eta}_\star^{\text{opc}}| \leq \frac{C_1}{1-\gamma}|\mathcal{A}|^{\frac{1}{4}} C_2^T \sqrt{T}\bar{\sigma}_\pi. \tag{8}$$

Proof. From combining Lemmas 5 and 6 it follows that

$$|\eta - \tilde{\eta}_\star^{\text{opc}}| \leq \sqrt{2\sqrt{|\mathcal{A}|}(1+L_\pi^2)}\bar{\sigma}_\pi L_f L_r \sum_{t\geq 0}\gamma^t \sqrt{\sum_{t'=0}^{t}(L_f^2+L_\pi^2)^{t'}} \tag{50}$$

with the shorthand notations $C_1 = \sqrt{2(1+L_\pi^2)}L_f L_r$ and $C_2 = L_f^2 + L_\pi^2$

$$= C_1|\mathcal{A}|^{\frac{1}{4}}\bar{\sigma}_\pi \sum_{t=0}^{T}\gamma^t \sqrt{\sum_{t'=0}^{t} C_2^{t'}} \tag{51}$$

Since $t \leq T$, we have that $\sum_{t'=0}^{t} C_2^{t'} \leq TC_2^T$

$$\leq C_1|\mathcal{A}|^{\frac{1}{4}}\bar{\sigma}_\pi C_2^{\frac{T}{2}}\sqrt{T}\sum_{t=0}^{T}\gamma^t \tag{52}$$

Since $T \leq \infty$, we have with the geometric series $\sum_{t=0}^{T}\gamma^t \leq 1/(1-\gamma)$

$$\leq \frac{C_1}{1-\gamma}|\mathcal{A}|^{\frac{1}{4}}C_2^{\frac{T}{2}}\sqrt{T}\bar{\sigma}_\pi \tag{53}$$

□

A.4.3 Definitions, Helpful Identities and Supporting Lemmas

Here we briefly summarize some basic definitions and properties that will be used throughout the following.

- Wasserstein distance of sums of random variables (see, e.g., Mariucci et al. (2018, Corollary 1) for a proof):

$$\mathcal{W}_p(p_1 * \cdots * p_n, q_1 * \cdots * q_n) \leq \sum_{i=1}^{n}\mathcal{W}_p(p_i, q_i) \tag{54}$$

- For any function $g(\mathbf{z}, \hat{\mathbf{z}})$ we have

$$\iint p(\mathbf{s}_{t+1} - g(\mathbf{z}, \hat{\mathbf{z}}))\nu(\mathbf{z}, \hat{\mathbf{z}})\,\mathrm{d}\mathbf{z}\,\mathrm{d}\hat{\mathbf{z}} = p * \iint \delta(\mathbf{s}_{t+1} - g(\mathbf{z}, \hat{\mathbf{z}}))\nu(\mathbf{z}, \hat{\mathbf{z}})\,\mathrm{d}\mathbf{z}\,\mathrm{d}\hat{\mathbf{z}} \tag{55}$$

- For any multivariate random variable $\mathbf{z}_1$ and $\mathbf{z}_2$ with probability distributions $p(\mathbf{z}_1) = p_1(\mathbf{x})q(\mathbf{y})$ and $p(\mathbf{z}_2) = p_2(\mathbf{x})q(\mathbf{y})$, respectively, we have that (Panaretos & Zemel, 2019)

$$\mathcal{W}_2^2(p_1(\mathbf{x})q(\mathbf{y}), p_2(\mathbf{x})q(\mathbf{y})) = \mathcal{W}_2^2(p_1(\mathbf{x}), p_2(\mathbf{x})). \tag{56}$$

Further, the following Lemmas are helpful for the proof of Theorem 1.

Lemma 7 (Kantorovich-Rubinstein (cf. Mariucci et al. (2018) Proposition 1.3))**.** *Let X and Y be integrable real random variables. Denote by μ and μ their laws [...]. Then the following characterization of the Wasserstein distance of order 1 holds:*

$$\mathcal{W}_1(\nu, \mu) = \sup_{\|\phi\|_{\text{Lip}}\leq 1} \mathop{\mathbb{E}}_{x\sim\nu(\cdot)}[\phi(x)] - \mathop{\mathbb{E}}_{y\sim\mu(\cdot)}[\phi(y)], \tag{57}$$

where the supremum is being taken over all ϕ satisfying the Lipschitz condition $|\phi(x)-\phi(y)| \leq |x-y|$, for all $x, y \in \mathbb{R}$.

Lemma 8. *Let f be L_f-Lipschitz with respect to a metric d. Then*

$$|\mathop{\mathbb{E}}_{x\sim\nu(\cdot)}[f(x)] - \mathop{\mathbb{E}}_{y\sim\mu(\cdot)}[f(y)]| \leq L_f\mathcal{W}_1(\nu, \mu) \leq L_f\mathcal{W}_2(\nu, \mu) \tag{58}$$

Proof. The first inequality is a direct consequence of Lemma 7 and the second inequality comes from the well-known fact that if $1 \leq p \leq q$, then $\mathcal{W}_p(\mu, \nu) \leq \mathcal{W}_q(\mu, \nu)$ (cf. Mariucci et al. (2018, Lemma 1.2)). □

Lemma 9. *For any two functions $f(\mathbf{s})$ and $g(\mathbf{s})$ and probability density $p(\mathbf{s})$ that govern the distributions defined by*

$$p_1(\mathbf{x}_1) = \int \delta(\mathbf{x}_1 - f(\mathbf{s}))p(\mathbf{s})\,\mathrm{d}\mathbf{s} \quad \textit{and} \quad p_2(\mathbf{x}_2) = \int \delta(\mathbf{x}_2 - g(\mathbf{s}))p(\mathbf{s})\,\mathrm{d}\mathbf{s}, \tag{59}$$

it holds for any $q \geq 1$ that

$$\mathcal{W}_q^q\left(p_1, p_2\right) \leq \int \|f(\mathbf{s}) - g(\mathbf{s})\|^q p(\mathbf{s})\,\mathrm{d}\mathbf{s}. \tag{60}$$

Proof. We have

$$\mathcal{W}_q^q\left(p_1(\mathbf{x}_1), p_2(\mathbf{x}_2)\right) = \inf_{\gamma \in \Gamma(p_1, p_2)} \iint \|\xi_1 - \xi_2\|^q \gamma(\xi_1, \xi_2)\,\mathrm{d}\xi_1\,\mathrm{d}\xi_2 \tag{61}$$

Enforcing the following structure on $\gamma(\xi_1, \xi_2)$ reduces the space of possible distributions: $\gamma(\xi_1, \xi_2) = \int \delta(\xi_1 - f(\mathbf{s}))\delta(\xi_2 - g(\mathbf{s}))p(\mathbf{s})\,\mathrm{d}\mathbf{s}$, so that $\gamma(\xi_1, \xi_2) \in \Gamma(p_1, p_2)$ and thus

$$\leq \int \|\xi_1 - \xi_2\|^q \int \delta(\xi_1 - f(\mathbf{s}))\delta(\xi_2 - g(\mathbf{s}))p(\mathbf{s})\,\mathrm{d}\mathbf{s}\,\mathrm{d}\xi_1\,\mathrm{d}\xi_2 \tag{62}$$

Integrating over ξ_1 and ξ_2 yields

$$= \int \|f(\mathbf{s}) - g(\mathbf{s})\|^q p(\mathbf{s})\,\mathrm{d}\mathbf{s} \tag{63}$$

□

Lemma 10. *If the policy $\pi(\mathbf{a}_t \mid \mathbf{s}_t)$ is L_π-Lipschitz with respect to $\mathbf{s}_t$ under the Wasserstein distance, then with $p(\hat{\mathbf{s}}, \hat{\mathbf{a}}) = \pi(\hat{\mathbf{a}} \mid \hat{\mathbf{s}})p(\hat{\mathbf{s}})$ and $\tilde{p}(\mathbf{s}, \mathbf{a}) = \pi(\mathbf{a} \mid \mathbf{s})\tilde{p}(\mathbf{s})$,*

$$\mathcal{W}_2^2(p(\hat{\mathbf{s}}, \hat{\mathbf{a}}), \tilde{p}(\mathbf{s}, \mathbf{a})) \leq (1 + L_\pi^2)\mathcal{W}_2^2(p(\hat{\mathbf{s}}), \tilde{p}(\mathbf{s})) \tag{64}$$

Proof.

$$\mathcal{W}_2^2(p(\hat{\mathbf{s}}, \hat{\mathbf{a}}), \tilde{p}(\mathbf{s}, \mathbf{a})) \tag{65}$$

$$= \inf_{\gamma \in \Gamma(p(\hat{\mathbf{s}}, \hat{\mathbf{a}}), \tilde{p}(\mathbf{s}, \mathbf{a}))} \int \left[\|\hat{\mathbf{a}} - \mathbf{a}\|^2 + \|\hat{\mathbf{s}} - \mathbf{s}\|^2\right] \gamma(\hat{\mathbf{a}}, \mathbf{a}, \hat{\mathbf{s}}, \mathbf{s})\,\mathrm{d}\hat{\mathbf{a}}\,\mathrm{d}\mathbf{a}\,\mathrm{d}\hat{\mathbf{s}}\,\mathrm{d}\mathbf{s} \tag{66}$$

Enforcing the following structure on γ reduces the space of possible distributions: $\gamma(\hat{\mathbf{s}}, \mathbf{s}, \hat{\mathbf{a}}, \mathbf{a}) = \gamma(\hat{\mathbf{s}}, \mathbf{s})\gamma(\hat{\mathbf{a}}, \mathbf{a} \mid \hat{\mathbf{s}}, \mathbf{s})$ with $\gamma(\hat{\mathbf{s}}, \mathbf{s}) \in \Gamma(p(\hat{\mathbf{s}}), \tilde{p}(\mathbf{s}))$ and $\gamma(\hat{\mathbf{a}}, \mathbf{a}|\hat{\mathbf{s}}, \mathbf{s}) \in \Gamma(\pi(\hat{\mathbf{a}} \mid \hat{\mathbf{s}}), \pi(\mathbf{a} \mid \mathbf{s}))$.

$$\leq \inf_{\substack{\gamma(\hat{\mathbf{s}}, \mathbf{s}) \in \Gamma(p(\hat{\mathbf{s}}), \tilde{p}(\mathbf{s})) \\ \gamma(\hat{\mathbf{a}}, \mathbf{a}|\hat{\mathbf{s}}, \mathbf{s}) \in \Gamma(\pi(\hat{\mathbf{a}}|\hat{\mathbf{s}}), \pi(\mathbf{a}|\mathbf{s}))}} \int \left\{ \int \left[\|\hat{\mathbf{a}} - \mathbf{a}\|^2 \gamma(\hat{\mathbf{a}}, \mathbf{a} \mid \hat{\mathbf{s}}, \mathbf{s})\,\mathrm{d}\hat{\mathbf{a}}\,\mathrm{d}\mathbf{a}\right\} + \|\hat{\mathbf{s}} - \mathbf{s}\|^2\right] \gamma(\hat{\mathbf{s}}, \mathbf{s})\,\mathrm{d}\hat{\mathbf{s}}\,\mathrm{d}\mathbf{s} \tag{67}$$

Interchange infimum and the integral: Rockafellar (1976, Theorem 3A)

$$= \inf_{\gamma(\hat{\mathbf{s}}, \mathbf{s})} \int \left\{ \inf_{\gamma(\hat{\mathbf{a}}, \mathbf{a}|\hat{\mathbf{s}}, \mathbf{s})} \int \|\hat{\mathbf{a}} - \mathbf{a}\|^2 \gamma(\hat{\mathbf{a}}, \mathbf{a} \mid \hat{\mathbf{s}}, \mathbf{s})\,\mathrm{d}\hat{\mathbf{a}}\,\mathrm{d}\mathbf{a} + \|\hat{\mathbf{s}} - \mathbf{s}\|^2 \right\} \gamma(\hat{\mathbf{s}}, \mathbf{s})\,\mathrm{d}\hat{\mathbf{s}}\,\mathrm{d}\mathbf{s} \tag{68}$$

$$= \inf_{\gamma(\hat{\mathbf{s}}, \mathbf{s}) \in \Gamma(p(\hat{\mathbf{s}}), \tilde{p}(\mathbf{s}))} \int \left\{ \mathcal{W}_2^2(\pi(\hat{\mathbf{a}} \mid \hat{\mathbf{s}}), \pi(\mathbf{a} \mid \mathbf{s})) + \|\hat{\mathbf{s}} - \mathbf{s}\|^2 \right\} \gamma(\hat{\mathbf{s}}, \mathbf{s})\,\mathrm{d}\hat{\mathbf{s}}\,\mathrm{d}\mathbf{s} \tag{69}$$

Using the assumption that the action distribution is L_π-Lipschitz continuous under the Wasserstein metric with respect to the state $\mathbf{s}$:

$$\leq \inf_{\gamma(\hat{\mathbf{s}}, \mathbf{s}) \in \Gamma(p(\hat{\mathbf{s}}), \tilde{p}(\mathbf{s}))} \int (1 + L_\pi^2)\|\hat{\mathbf{s}} - \mathbf{s}\|^2] \gamma(\hat{\mathbf{s}}, \mathbf{s})\,\mathrm{d}\hat{\mathbf{s}}\,\mathrm{d}\mathbf{s} \tag{70}$$

$$= (1 + L_\pi^2)\mathcal{W}_2^2(p(\hat{\mathbf{s}}), \tilde{p}(\mathbf{s})) \tag{71}$$

□

Lemma 11 (Average Squared Euclidean Distance Between Actions)**.** *If the policy $\pi(\mathbf{a} \mid \mathbf{s})$ is L_π-Lipschitz with respect to $\mathbf{s}$ under the Wasserstein distance and the policy's (co-)variance $\mathrm{Var}[\pi(\mathbf{a} \mid \mathbf{s})] = \Sigma_\pi(\mathbf{s}) \in \mathbb{S}_+^{|\mathcal{A}|}$ is finite over the complete state space, i.e., $\max_{\mathbf{s}\in\mathcal{S}} \mathrm{trace}\{\Sigma_\pi(\mathbf{s})\} \leq \bar{\sigma}_\pi^2$, then*

$$\mathop{\mathbb{E}}_{\substack{\hat{\mathbf{a}}_t \sim \pi(\hat{\mathbf{s}}_t) \\ \mathbf{a}_t \sim \pi(\mathbf{s}_t)}} \left[\|\hat{\mathbf{a}}_t - \mathbf{a}_t\|^2 \right] \leq L_\pi^2 \|\hat{\mathbf{s}}_t - \mathbf{s}_t\|^2 + 2\sqrt{|\mathcal{A}|}\bar{\sigma}_\pi^2 \tag{72}$$

Proof. Straightforward application of Corollary 1 and Lemma 13 □

Lemma 12 (Average Squared Euclidean Distance)**.** *Consider two random variables $\mathbf{x}, \mathbf{y}$ with distributions $p_\mathbf{x}, p_\mathbf{y}$, mean vectors $\mu_\mathbf{x}, \mu_\mathbf{y} \in \mathbb{R}^m$ and covariance matrices $\Sigma_\mathbf{x}, \Sigma_\mathbf{y} \in \mathbb{S}_+^m$, respectively. Then the average squared Euclidean distance between the two is*

$$\mathop{\mathbb{E}}_{\mathbf{x},\mathbf{y}} \left[\|\mathbf{x} - \mathbf{y}\|^2 \right] = \|\mu_\mathbf{x} - \mu_\mathbf{y}\|^2 + \mathrm{trace}\left\{\Sigma_\mathbf{x} + \Sigma_\mathbf{y}\right\}. \tag{73}$$

Proof. Define $\mathbf{z} = \mathbf{x} - \mathbf{y}$ with mean $\mu_\mathbf{z} = \mu_\mathbf{x} - \mu_\mathbf{y}$ and variance $\Sigma_\mathbf{z} = \Sigma_\mathbf{x} + \Sigma_\mathbf{y}$.

$$\begin{aligned}
\mathbb{E}\left[\|\mathbf{z}\|^2\right] &= \mathbb{E}\left[\sum_i \mathbf{z}_i^2\right] \\
&= \sum_i \mathbb{E}\left[\mathbf{z}_i^2\right] \\
&= \sum_i \mathbb{E}[\mathbf{z}_i]^2 + \mathrm{Var}[\mathbf{z}_i] \\
&= \mu_\mathbf{z}^\top \mu_\mathbf{z} + \mathrm{trace}\left\{\Sigma_\mathbf{z}\right\} \\
&= \|\mu_\mathbf{x} - \mu_\mathbf{y}\|^2 + \mathrm{trace}\left\{\Sigma_\mathbf{x} + \Sigma_\mathbf{y}\right\}.
\end{aligned}$$

□

Theorem 2 (Gelbrich Bound (from Kuhn et al. (2019)))**.** *If $\|\cdot\|$ is the Euclidean norm, and the distributions $p_\mathbf{x}$ and $p_\mathbf{y}$ have mean vectors $\mu_\mathbf{x}, \mu_\mathbf{y} \in \mathbb{R}^m$ and covariance matrices $\Sigma_\mathbf{x}, \Sigma_\mathbf{y} \in \mathbb{S}_+^m$, respectively, then*

$$\mathcal{W}_2(p_\mathbf{x}, p_\mathbf{y}) \geq \sqrt{\|\mu_\mathbf{x} - \mu_\mathbf{y}\|^2 + \mathrm{trace}\left\{\Sigma_\mathbf{x} + \Sigma_\mathbf{y} - 2\left(\Sigma_\mathbf{x}^{1/2}\Sigma_\mathbf{y}\Sigma_\mathbf{x}^{1/2}\right)^{1/2}\right\}}. \tag{74}$$

The bound is exact if $p_\mathbf{x}$ and $p_\mathbf{y}$ are elliptical distributions with the same density generator.

Corollary 1. *Consider the same setting as in Lemma 12, then the average squared Euclidean distance is bounded by*

$$\mathop{\mathbb{E}}_{\mathbf{x},\mathbf{y}} \left[\|\mathbf{x} - \mathbf{y}\|^2 \right] \leq \mathcal{W}_2^2(p_\mathbf{x}, p_\mathbf{y}) + 2\,\mathrm{trace}\left\{\left(\Sigma_\mathbf{x}^{1/2}\Sigma_\mathbf{y}\Sigma_\mathbf{x}^{1/2}\right)^{1/2}\right\}. \tag{75}$$

Proof. Straightforward application of the results from Lemma 12 and Theorem 2. □

Lemma 13. *If the policy's (co-)variance $\mathrm{Var}[\pi(\mathbf{a} \mid \mathbf{s})] = \Sigma_\pi(\mathbf{s}) \in \mathbb{S}_+^{|\mathcal{A}|}$ is finite over the complete state space, i.e., $\max_{\mathbf{s}\in\mathcal{S}} \mathrm{trace}\{\Sigma_\pi(\mathbf{s})\} \leq \bar{\sigma}_\pi^2$, then*

$$\mathrm{trace}\left\{\left(\Sigma_\pi(\hat{\mathbf{s}})^{1/2}\Sigma_\pi(\mathbf{s})\Sigma_\pi(\hat{\mathbf{s}})^{1/2}\right)^{1/2}\right\} \leq \sqrt{|\mathcal{A}|}\bar{\sigma}_\pi^2 \tag{76}$$

Proof.

$$\mathrm{trace}\left\{\left(\Sigma_\pi(\hat{\mathbf{s}})^{1/2}\Sigma_\pi(\mathbf{s})\Sigma_\pi(\hat{\mathbf{s}})^{1/2}\right)^{1/2}\right\} \tag{77}$$

The trace of a matrix is the same as the sum of its eigenvalues, and the square root of a matrix has eigenvalues that are square root of its eigenvalues. From Jensen's inequality we know that $\sum_{i=1}^{|\mathcal{A}|} \sqrt{\lambda_i} \leq \sqrt{|\mathcal{A}| \sum_{i=1}^{|\mathcal{A}|} \lambda_i}$ and consequently it holds for a matrix $\mathbf{M} \in \mathbb{R}^{|\mathcal{A}|\times|\mathcal{A}|}$ that $\mathrm{trace}\{\mathbf{M}^{1/2}\} \leq \sqrt{|\mathcal{A}|\,\mathrm{trace}\{\mathbf{M}\}}$, so that

$$\leq \sqrt{|\mathcal{A}|\,\mathrm{trace}\{\Sigma_\pi(\hat{\mathbf{s}})^{1/2}\Sigma_\pi(\mathbf{s})\Sigma_\pi(\hat{\mathbf{s}})^{1/2}\}} \tag{78}$$

The trace is invariant under cyclic permutation

$$= \sqrt{|\mathcal{A}| \operatorname{trace}\{\Sigma_\pi(\hat{\mathbf{s}})\Sigma_\pi(\mathbf{s})\}} \tag{79}$$

Since both matrices are positive semi-definite, it follows from the Cauchy-Schwartz inequality that

$$\leq \sqrt{|\mathcal{A}| \operatorname{trace}\{\Sigma_\pi(\hat{\mathbf{s}})\} \operatorname{trace}\{\Sigma_\pi(\mathbf{s})\}} \tag{80}$$

By assumption, the covariance matrices' traces are bounded

$$\leq \sqrt{|\mathcal{A}|}\bar{\sigma}_\pi^2 \tag{81}$$

□

B MOTIVATING EXAMPLE – IN-DEPTH ANALYSIS

In this section, we re-visit the motivating example presented in Section 4.1 of the main paper. For completeness, we re-state all assumptions that lead to the simplified system at hand. We continue with an analysis of the reward landscape and how OPC influences its shape. Next, we investigate how an increasing mismatch of the dynamics model impacts the gradient error. In addition to the result presented in the main paper, we here show the influence of different model errors, i.e., $\Delta\mathbf{A}$ as well as $\Delta\mathbf{B}$. While OPC is motivated for the use case of on-policy RL algorithms, we further show that the resulting gradients are robust with respect to differences in data-generating and evaluation policy, i.e., the off-policy setting. Lastly, we state the the signed gradient distance that we use for evaluation of the gradient errors, state the relevant theorem for determining the closed-loop stability of linear systems, as well as all numerical values used for the motivating example.

B.1 SETUP

Here, we assume a linear system with deterministic dynamics

$$p(\mathbf{s}_{t+1} \mid \mathbf{s}_t, \mathbf{a}_t) = \delta(\mathbf{A}\mathbf{s}_t + \mathbf{B}\mathbf{a}_t \mid \mathbf{s}_t, \mathbf{a}_t), \quad \rho_0(\mathbf{s}_0) = \delta(\mathbf{s}_0) \tag{82}$$

with $\mathbf{A}, \mathbf{B} \in \mathbb{R}$ and $\delta(\cdot)$ denoting the Dirac-delta distribution. The linear policy and bell-shaped reward are given by the following equations

$$\pi_\theta(\mathbf{a}_t \mid \mathbf{s}_t) = \delta(\theta\mathbf{s}_t \mid \mathbf{s}_t) \text{ with } \theta \in \mathbb{R} \quad \text{and} \quad r(\mathbf{s}_t, \mathbf{a}_t) = \exp\left\{-\left(\frac{\mathbf{s}_t}{\sigma_r}\right)^2\right\}. \tag{83}$$

Further, we assume to have access to an approximate dynamics model $\tilde{p}$

$$\tilde{p}(\mathbf{s}_{t+1} \mid \mathbf{s}_t, \mathbf{a}_t) = \delta((\mathbf{A} + \Delta\mathbf{A})\mathbf{s}_t + (\mathbf{B} + \Delta\mathbf{B})\mathbf{a}_t \mid \mathbf{s}_t, \mathbf{a}_t), \tag{84}$$

where $\Delta\mathbf{A}, \Delta\mathbf{B}$ quantify the mismatch between the approximate model and the true system. For completeness, the (deterministic) policy gradient is defined as

$$\nabla_\theta \frac{1}{T} \sum_{t=0}^{T-1} r(\mathbf{s}_t, \mathbf{a}_t), \tag{85}$$

where the state/action pairs are obtained by simulating any of the two above models for T time-steps and following policy π_θ^n resulting in the trajectory $\tilde{\tau}^n = \{(\mathbf{s}_t^n, \mathbf{a}_t^n)\}_{t=0}^{T-1}$. Because both the model and policy are deterministic, we can compute the analytical policy gradient from only one rollout.

B.2 REWARD LANDSCAPES

In a first step, we will look at the cumulative rewards as a function of the policy parameter for the different systems at hand: 1) the true system, 2) the approximate model without OPC and 3) the approximate model with OPC. Further, let's assume that the model mismatch is fixed to some arbitrary value. The resulting reward landscapes are shown in Fig. 7. We would like to emphasize several key aspects in the plots: First, as one would expect the model mismatch leads to different optimal policies as well as misleading policy gradients for large parts of the policy parameter space. Second, the reward landscape for the model with OPC depends on the respective reference policy π^n that was used to generate the data for the corrections. Consequently, the correct reward is recovered at $\theta = \theta^n$. More importantly, the OPC reshape the reward landscape such that the policy gradients point towards the correct optimum (left plot). Lastly, even when using OPC the policy gradient's sign is not guaranteed to have the correct sign (right plot). The extent of this effect strongly depends on the model mismatch, which we will investigate in the next section.

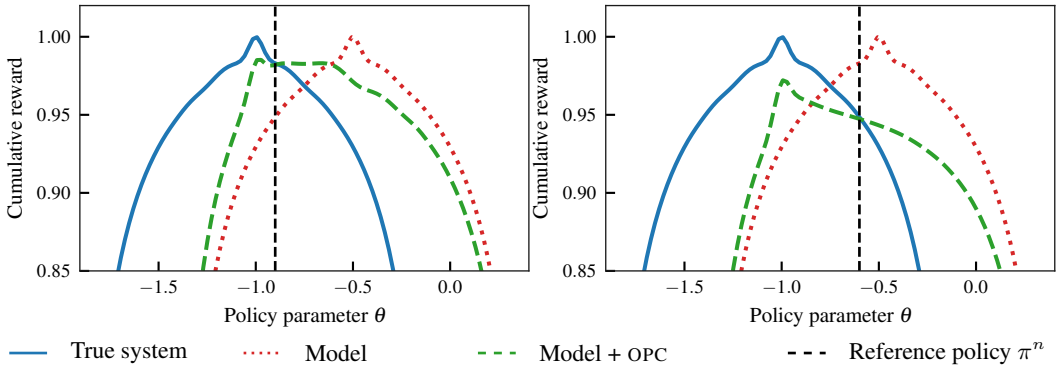

Figure 7: Cumulative reward for different systems as a function of the policy parameter. The reference trajectory that is used for OPC was generated by π_θ^n (denoted by the black dashed line). The model mismatch between the true system and the approximated model is $\Delta\mathbf{A} = 0.5, \Delta\mathbf{B} = 0.0$.

B.3 Influence of Model Error

As shown in the previous section, the estimated policy gradient depends on the current policy as well as the mismatch between the true system and the approximate model. Fig. 2 depicts the (signed) differences between the true policy gradient as well as the approximated gradient as a function of model mismatch and the reference policy. Here, the opacity of the background denotes the magnitude of the error and the color denotes if the true and estimated gradient have the same (blue) or oppposite (red) sign. In the context of policy learning, the sign of the gradient is more relevant than the actual magnitude due to internal re-scaling of the gradients in modern implementations of stochastic optimizers such as Adam (Kingma & Ba, 2015). In our example, even for negligible model errors (either in $\Delta\mathbf{A}$ or $\Delta\mathbf{B}$), the model-based approach can lead to gradient estimates with the opposite sign, indicated by the large red areas for the left figures in Fig. 2. On the other hand, applying OPC to the model, we gradient estimates are significantly more robust with respect to errors in the dynamics.x

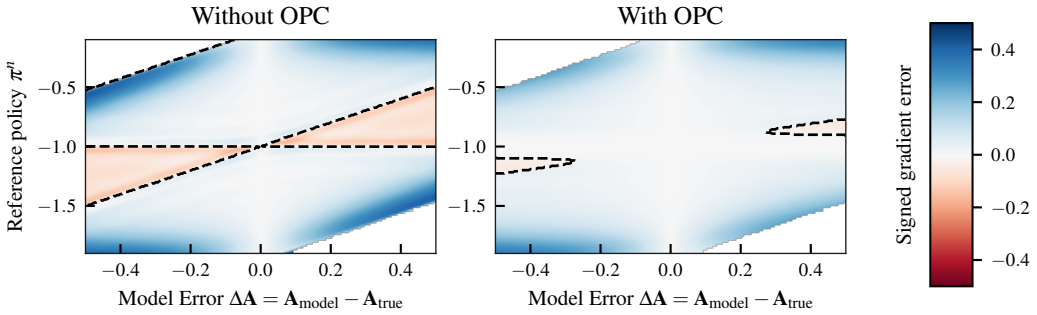

(a) Gradient error when varying model error $\Delta\mathbf{A}$

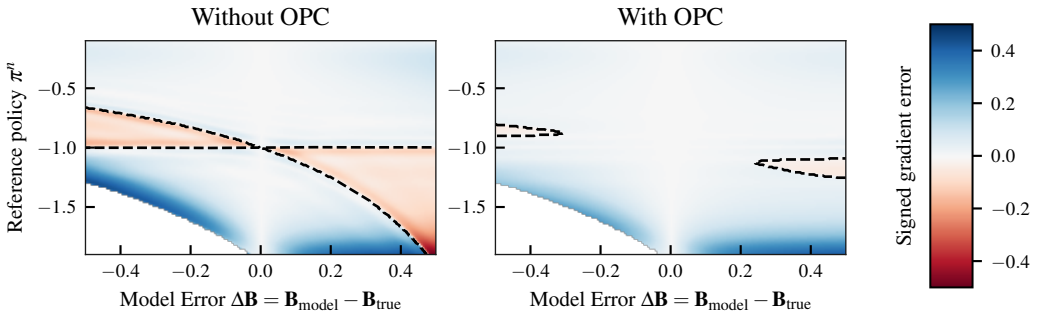

(b) Gradient error when varying model error $\Delta\mathbf{B}$

Figure 8: Signed gradient error (see Equation equation 86) when using the approximate model to estimate the policy gradient without (left) and with (right) on-policy corrections (OPCs). Using OPCs increases the robustness of the gradient estimate with respect to the model error.

B.4 Influence of Off-Policy Error

Until now we have considered the case in which the reference trajectory used for OPC is generated with the same policy as the one used for gradient estimation, i.e., the on-policy setting. In this case, we have observed that the true return could be recovered (see Fig. 7) when using OPC and that the gradient estimates are less sensitive to model errors (see Fig. 8). The off-policy case corresponds to the policy gains in Fig. 7 that are different from the reference policy π^n indicated by the dashed line. Fig. 9 summarizes the results for the off-policy setting. Here, we varied the policy error and the reference policy itself for varying model errors. Note that for the correct model, we always recover the true gradient. But also for inaccurate models, the gradient estimates retain a good quality in most cases, with the exception for some model/policy combinations that are close to unstable.

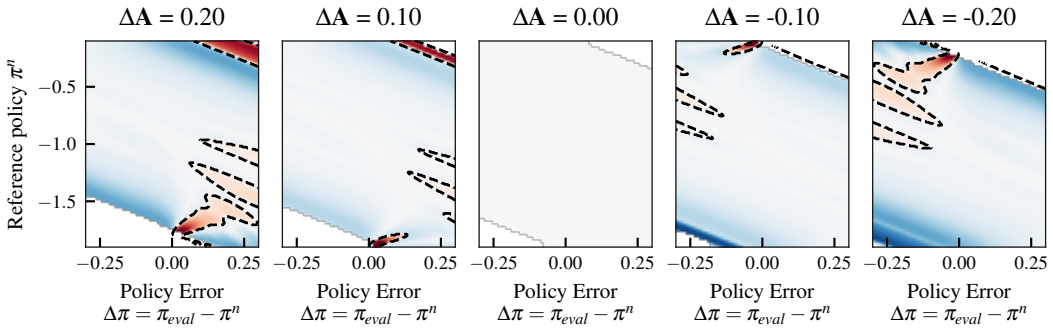

(a) Model error $\Delta\mathbf{A}$.

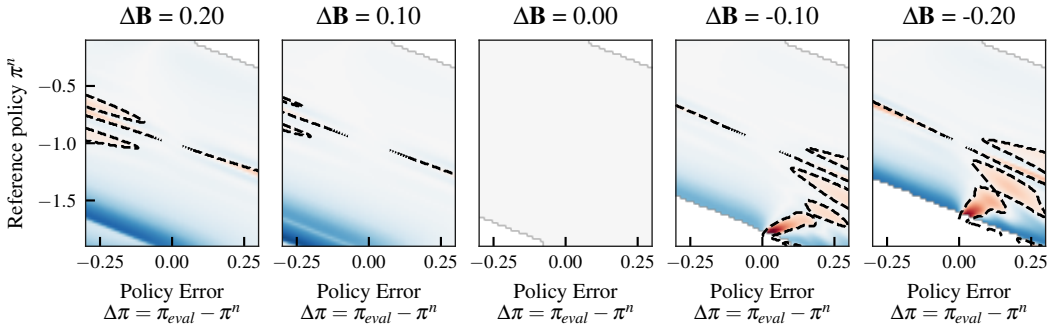

(b) Model error $\Delta\mathbf{B}$.

Figure 9: Signed gradient error due to off-policy data when using OPC. Note that we retain the true gradient in case of no model error.

B.5 Additional Information

Next, we provide some additional information about how we compute gradient distances, properties of linear systems, and exact numerical values used.

B.5.1 Computing the Signed Gradient Distance

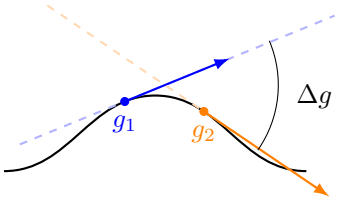

Figure 10: Sketch depicting the signed gradient distance Eq. (86). In this particular case, gradient g_1 is positive and g_2 is negative.

In order to compare two (1-dimensional) gradients in terms of sign and magnitude, we use the following formula

$$d(g_1, g_2) = \frac{1}{\pi} \begin{cases} \text{sign}(g_2) \cdot \Delta g, & \text{if } g_1 = 0 \\ \text{sign}(g_1) \cdot \Delta g, & \text{if } g_2 = 0 \\ \text{sign}(g_1 \cdot g_2) \cdot \Delta g, & \text{otherwise} \end{cases}, \quad \text{with} \quad \Delta g = |\arctan g_1 - \arctan g_2| \,. \tag{86}$$

The magnitude of this quantity depends on the normalized difference between the tangent's angles Δg and is positive for gradients with the same sign and vice versa it is negative for gradients with opposing signs. See also Fig. 10 for a sketch.

B.5.2 DETERMINING THE CLOSED-LOOP STABILITY FOR LINEAR SYSTEMS

For linear and deterministic systems, we can easily check if the system is (asymptotically) stable for a particular linear policy using the following standard result from linear system theory:

Theorem 3 (Exponential stability for linear time-invariant systems (Callier & Desoer, 1991))**.** *The solution of* $\mathbf{x}_{t+1} = \mathbf{F}\mathbf{x}_t$ *is exponentially stable if and only if* $\sigma(\mathbf{F}) \subset D(0,1)$*, i.e., every eigenvalue of* $\mathbf{F}$ *has magnitude strictly less than one.*

In our setting, this means that the closed-loop systems fulfilling the following are *unstable*,

$$|\mathbf{A} + \Delta\mathbf{A} + (\mathbf{B} + \Delta\mathbf{B})\theta| > 1, \tag{87}$$

i.e., the state and input grow exponentially. We therefore refrain from including unstable system in the results to avoid numerical issues for the gradients' computation. The respective areas in the plots are not colored, see e.g., bottom left corner in Fig. 8b.

B.5.3 NUMERICAL VALUES

The numerical values for all parameters used in the motivating example are given as follows:

- True system dynamics: $\mathbf{A} = 1.0, \mathbf{B} = 1.0$
- Initial condition: $\mathbf{s}_0 = 1.0$
- Reward width parameter: $\sigma_r = 0.05$
- Optimal policy gain: $\theta^* = -1.0$
- Rollout horizon: $T = 60$

C ADDITIONAL EXPERIMENTAL RESULTS

In this section, we provide additional experimental results that did not fit into the main body of the paper.

C.1 COMPARISON WITH OTHER BASELINE ALGORITHMS

Fig. 11 shows our method compared to a range of baseline algorithms. The results for all baselines were obtained from Janner et al. (2019) via personal communication. Note that all results are presented in terms of mean and standard deviation. The comparison includes the following methods:

- MBPO (Janner et al., 2019),
- PETS (Chua et al., 2018),
- SAC (Haarnoja et al., 2018),
- PPO (Schulman et al., 2017),
- STEVE (Buckman et al., 2018),
- SLBO (Luo et al., 2018).

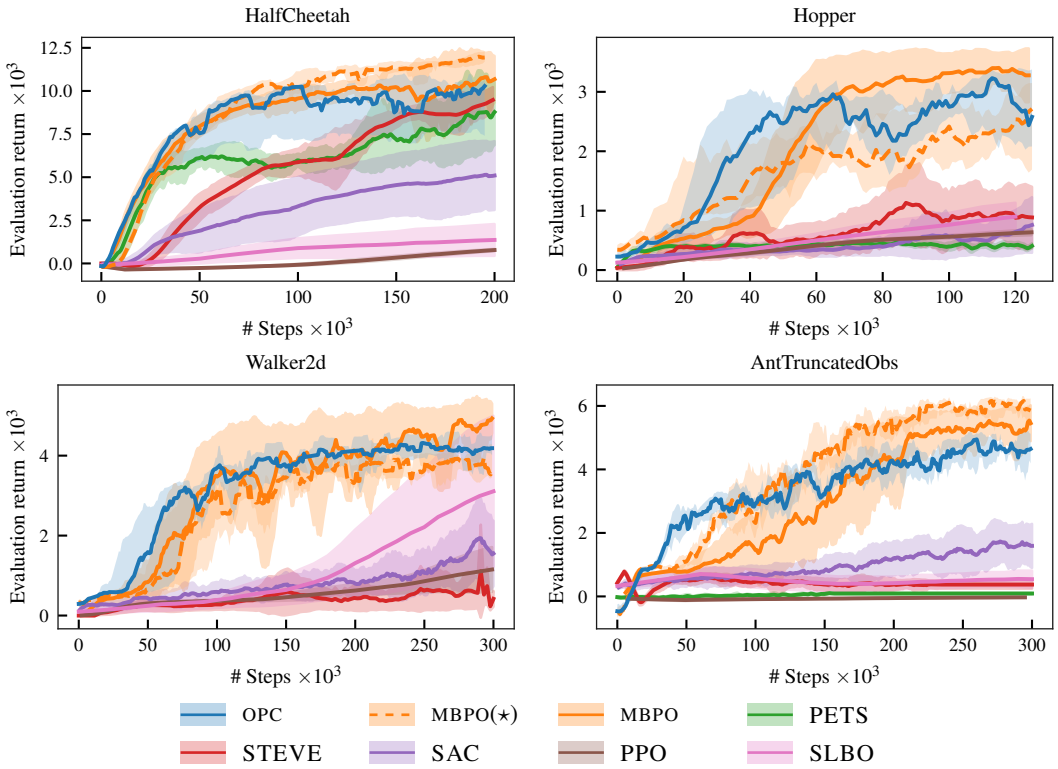

Figure 11: Comparison of OPC against a range of baseline methods on three MuJoCo environments. We present the mean and standard deviation across 5 independent experiments (10 for OPC and MBPO(⋆)). The original data for MBPO and the other baselines were provided by Janner et al. (2019).

C.2 Ablation - Retain Epochs

One of the hyperparameters that we found is critical to both OPC and MBPO(⋆), is `retain epochs`, i.e., the number of epochs that are kept in the data buffer for the simulated data generated with the $\tilde{p}^{\mathrm{x}}$ with $\mathrm{x} = \{\mathrm{OPC}, \mathrm{model}\}$. The results for a comparison are shown in Fig. 12. For MBPO(⋆), we found that for some environments (HalfCheetah, AntTruncatedObs) smaller values for `retain epochs` are helpful, i.e., simulated data is almost only on-policy, and for other environments larger values are beneficial (Hopper, Walker2d). For OPC on the other hand, we found that `retain epochs` $= 50$ almost always leads to better results.

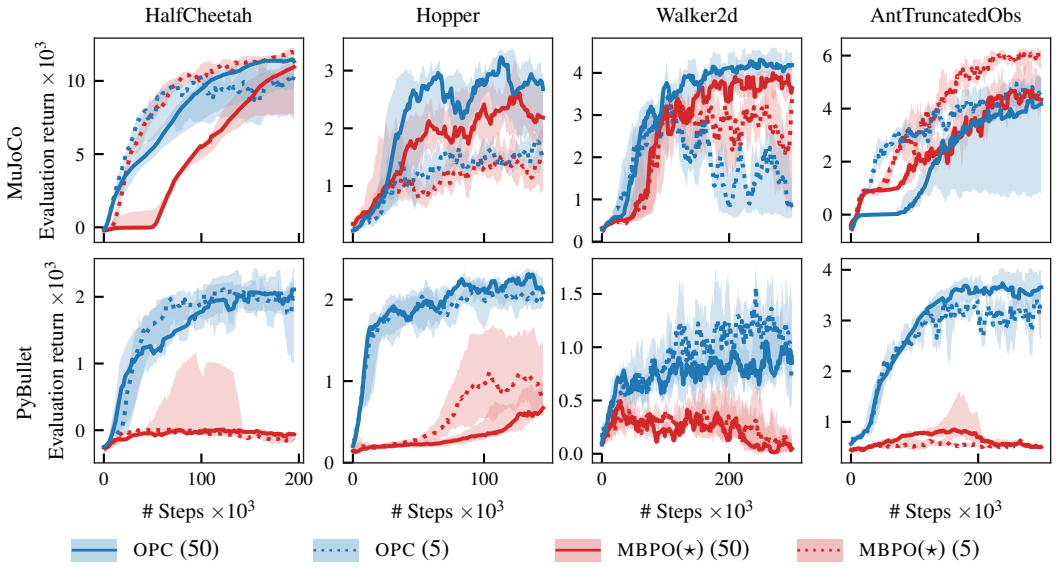

Figure 12: Ablation study for OPC and MBPO($\star$) on four environments from the MuJoCo control suite (top row) and their respective PyBullet implementations (bottom row). We vary the `retain epochs` hyperparameter (indicated by the number in the parentheses behind the legend entries), i.e., the number of epochs that are kept in the data buffer for the simulated data.

C.3 Implementation Changes to Original MBPO

Here, we provide details to the changes we made to the original implementation of MBPO. We denote our variant as MBPO($\star$).

Episodic Setting MBPO updates the policy during rollouts on the real environment. Algorithms 2 and 3 show the original and our version of MBPO, respectively. While the original version might be more sample efficient because it allows for more policy gradient updates based on more recent data, it is not realistic to update the policy during a rollout on the real environment.

Mix-in of Real Data As mentioned in the main paper, one of the key problems with model-based RL (MBRL) is that the generated data might exhibit so-called model-bias. Biased data can be problematic for policy optimization as the transition tuples possibly do not come from the true state distribution of the real environment, thus misleading the RL algorithm. In the original implementation of MBPO, the authors use a mix of simulated data from the model as well as observed data from the true environment for policy optimization (`https://github.com/JannerM/mbpo/blob/master/mbpo/algorithms/mbpo.py#L430`) to alleviate the issue of model bias. While this design choice might help in practice, it adds an additional hyperparameter and the exact influence of this parameter is difficult to interpret. We therefore refrain from mixing in data from the true environment but instead only use simulated transition tuples – staying true to the spirit of MBRL.

Fix Replay Buffer The replay buffer that stores the simulated data $\mathcal{D}_{\text{model}}$ for policy optimization is allocated to a fixed size of `rollout length`×`rollout batch size`×`retain epochs`, meaning that per epoch `rollout length` × `rollout batch size` transition tuples are simulated and only the data from the last `retain epochs` are kept in the buffer (`https://github.com/JannerM/mbpo/blob/master/mbpo/algorithms/mbpo.py#L351`). As the buffer is implemented as a FIFO queue and rollouts might terminate early such that the actual number of simulated transitions is less than `rollout length`, data from older episodes as specified by `retain epochs` are retained in the buffer. We assume that this is not the intended behaviour and correct for that in our implementation.

Algorithm 2 Original MBPO algorithm

Initialize policy π_ϕ, predictive model p_θ, environment dataset $\mathcal{D}_{\text{env}}$, model dataset $\mathcal{D}_{\text{model}}$
for N epochs **do**
  Train model p_θ on $\mathcal{D}_{\text{env}}$ via maximum likelihood
  for E steps **do**
    Take action in environment according to π_ϕ; add to $\mathcal{D}_{\text{env}}$
    for M model rollouts **do**
      Sample s_t uniformly from $\mathcal{D}_{\text{env}}$
      Perform k-step model rollout starting from s_t using policy π_ϕ; add to $\mathcal{D}_{\text{model}}$
    for G gradient updates **do**
      Update policy parameters on model data: $\phi \leftarrow \phi - \lambda_\pi \hat{\nabla}_\phi J_\pi(\phi, \mathcal{D}_{\text{model}})$

Algorithm 3 Our version of MBPO algorithm, denoted as MBPO($\star$)

Initialize policy π_ϕ, predictive model p_θ, environment dataset $\mathcal{D}_{\text{env}}$, model dataset $\mathcal{D}_{\text{model}}$
for N epochs **do**
  Train model p_θ on $\mathcal{D}_{\text{env}}$ via maximum likelihood
  for E steps **do**
    Take action in environment according to π_ϕ; add to $\mathcal{D}_{\text{env}}$
  for M model rollouts **do**
    Sample s_t uniformly from $\mathcal{D}_{\text{env}}$
    Perform k-step model rollout starting from s_t using policy π_ϕ; add to $\mathcal{D}_{\text{model}}$
  for G gradient updates **do**
    Update policy parameters on model data: $\phi \leftarrow \phi - \lambda_\pi \hat{\nabla}_\phi J_\pi(\phi, \mathcal{D}_{\text{model}})$

C.4 Results for Original MBPO Implementation

The following results were obtained with the original MBPO implementation without the changes described in Appendix C.3. Consequently, the results for OPC in this section also do not include these changes.

Comparative Evaluation

We evaluate the original implementation on three continuous control benchmark tasks from the MuJoCo control suite (Todorov et al., 2012). The results for OPC, two variants of MBPO and SAC are presented in Fig. 3. Both OPC and MBPO use a rollout horizon of $H = 10$ to generate the training data. The difference between the two MBPO variants lies in the mix-in ratio β of real off-policy transitions to the simulated training data. Especially for highly stochastic environments such as the Hopper, this mix-in ratio is a critical hyperparameter that requires careful tuning (see also Fig. 14). Fig. 3 indicates that OPC is on par with MBPO on both the InvertedPendulum and HalfCheetah environments that exhibit little stochasticity. On the Hopper environment, OPC outperforms both MBPO variants. Note that the mix-in ratio for MBPO is critical for successful learning (the original implementation uses $\beta = 5\%$). OPC on the other hand, does not require any mixed-in real data. SAC learns slower on the more complex Hopper and HalfCheetah environments, re-iterating that model-based approaches are significantly more data-efficient than model-free methods.

Large Ablation Study – Hopper

The full study investigates the influence of the following hyperparameters and design choices:

- Rollout length H and total number of simulated transitions N.
- Mix-in ratio of real transitions into the training data β.
- Deterministic or stochastic rollouts (for MBPO): Current state-of-the-art methods in MBRL rely on probabilistic dynamic models to capture both aleatoric and epistemic uncertainty. Accordingly, when rolling out the model, these two sources of uncertainty are accounted for. However, we show that in terms of evaluation return, the stochastic rollouts do not always lead to the best outcome.

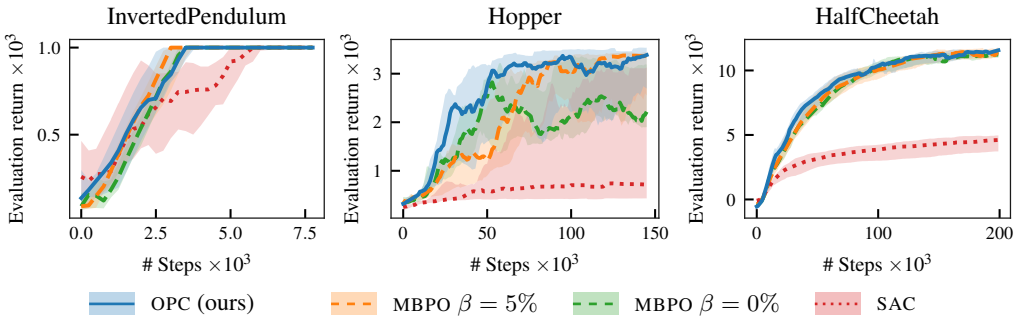

Figure 13: Results based on original implementation Appendix C.4: Comparison of OPC to the model-based MBPO and model-free SAC algorithms. The two MBPO variants differ in terms of the mix-in ratio β of real off-policy transitions in the training data – a critical hyperparameter. All model-based approaches outperform SAC in terms of convergence for the high-dimensional tasks. Moreover, on the highly stochastic Hopper environment, OPC outperforms both MBPO variants and does not require additional real off-policy data.

- Re-setting the buffer of simulated data after a policy optimization step: We found that re-setting the replay buffer for simulated data after each iteration of Algorithm 2 can have a large influence. In particular, the replay buffer is implemented as a FIFO queue with a fixed size. Hence, if the buffer is not emptied after each iteration, it still contains (simulated) off-policy transitions.

Fig. 14 presents the results of the ablation study. We want to highlight a few core insights:

1. When choosing the best setting for each method, OPC improves MBPO by a large margin (bottom row right). Generally, for long rollouts $H = 20$ (bottom row), OPC improves MBPO.
2. Across all settings, OPC performs well and is more robust with respect to the choices of hyperparameters (e.g., bottom row left and center, third row left). Only for few exceptions, re-setting the buffer can have detrimental effects (e.g., top right, third row right).
3. Mixing in real transition data can be highly beneficial for MBPO (second row left and center) but it can also have the opposite effect (bottom row).
4. Using deterministic rollouts can be beneficial (third row right and left), detrimental (third row center) or have no influence (bottom row left) for MBPO.
5. It is not clear, if re-setting the buffer after each iteration should overall be recommended or not. This remains an open question left for future research.

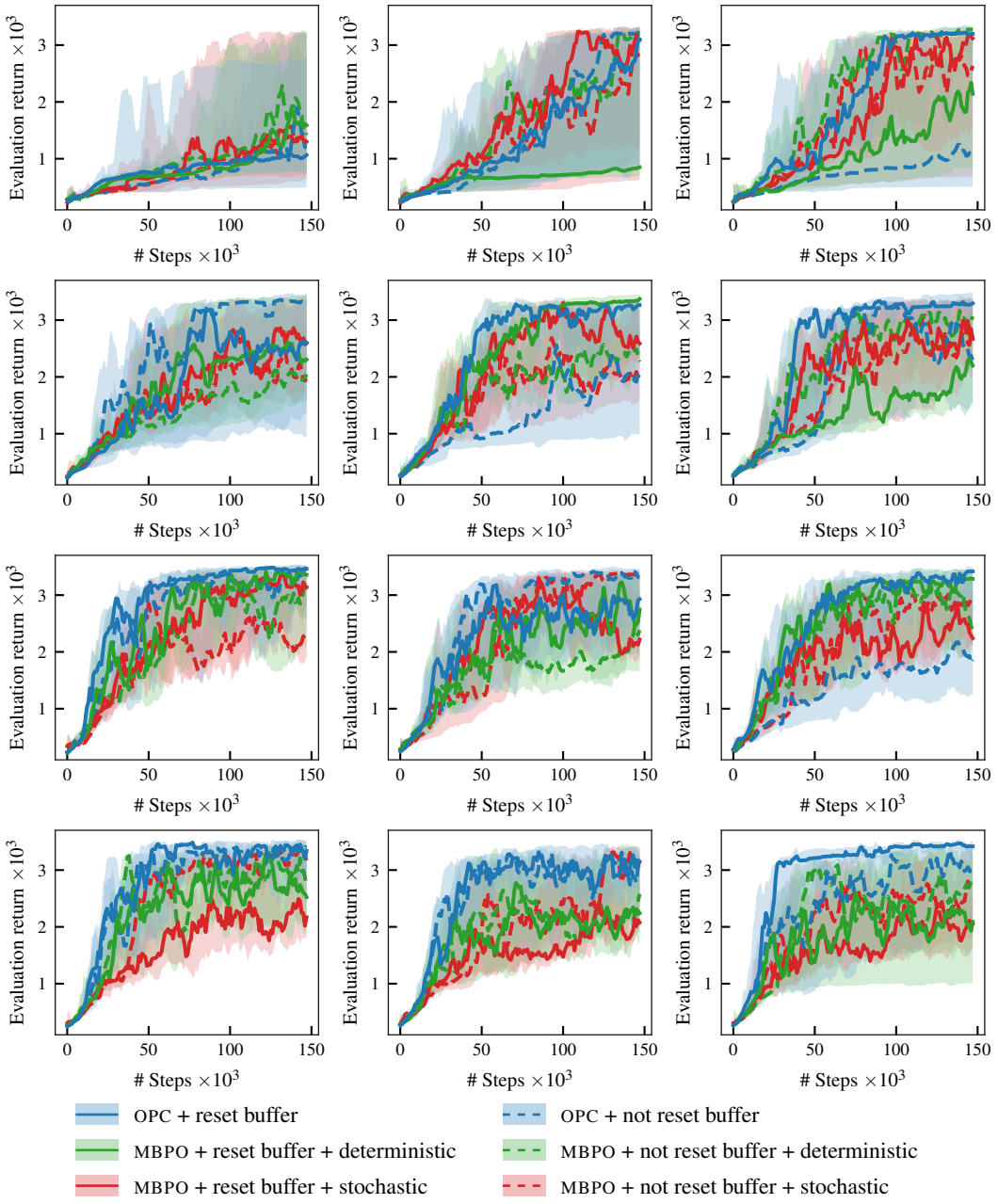

Figure 14: Results based on original implementation Appendix C.4: Large ablation study on the Hopper environment, investigating the influence various hyperparameters and design choices. Mix-in ratio of real data β (columns): $0\%, 5\%, 10\%$ from left to right. Rollout length H (rows): $1, 5, 10, 20$ from top to bottom.

D CONNECTION BETWEEN MBRL AND ILC

In this section we compare optimization-based or so-called *norm-optimal* ILC (NO-ILC) with MBRL. In particular, we show that under certain assumptions we can reduce the MBRL setting to NO-ILC. This comparison is structured as follows: First, we review the basic assumptions and notations for NO-ILC. While there are many variations on NO-ILC, we will only consider the very basic setting, i.e., linear dynamics, fully observed state and deterministic state evolution. Then, based on the lifted state representation of the problem, we derive the solution to the optimization problem that leads to the input sequence of the next iteration / rollout. Next, we will state the general MBRL problem and pose the simplifications that we need to make in order to be equivalent to the NO-ILC problem. Last, we show that the solution to the reduced MBRL problem is equivalent to the one of NO-ILC.

D.1 NORM-OPTIMAL ILC

The goal of NO-ILC is to find a sequence of inputs $\mathbf{a} = [\mathbf{a}_0^\top, \dots, \mathbf{a}_{T-1}^\top]^\top$ with length $T+1$ such that the outputs $\mathbf{y} = [\mathbf{y}_0^\top, \dots, \mathbf{y}_T^\top]^\top$ follow a desired output trajectory $\hat{\mathbf{y}} = [\hat{\mathbf{y}}_0^\top, \dots, \hat{\mathbf{y}}_T^\top]^\top$. In the simplest setting we assume that the system evolves according to the following linear dynamics

$$\mathbf{s}_{t+1} = \mathbf{A}\mathbf{s}_t + \mathbf{B}\mathbf{a}_t + \mathbf{d}_t \tag{88}$$

$$\mathbf{y}_t = \mathbf{C}\mathbf{s}_t, \tag{89}$$

with state $\mathbf{s}_t \in \mathbb{R}^{|\mathcal{S}|}$, action $\mathbf{a}_t \in \mathbb{R}^{|\mathcal{A}|}$, output $\mathbf{y}_t \in \mathbb{R}^p$ and disturbance $\mathbf{d}_t \in \mathbb{R}^{|\mathcal{S}|}$. One of the major assumption in ILC is that the disturbances $\mathbf{d}_t$ are *repetitive*, meaning that the sequence $\mathbf{d} = [\mathbf{d}_0^\top, \dots, \mathbf{d}_T^\top]^\top$ does not change (or only varies slightly) across multiple rollouts. While these disturbances can be considered to come from some exogenous error source, one can also interpret these as unmodeled effects of the dynamics, e.g., nonlinearities stemming from friction, aerodynamic effects, etc.

For the derivation, let's assume $\mathbf{C} = \mathbf{I}$ so that we're operating on an MDP. Consequently, the goal of ILC is to track a sequence of desired states $\hat{\mathbf{s}}$ instead of outputs $\hat{\mathbf{y}}$. In order to find an optimal input sequence, we minimize the squared 2-norm of a state's deviation from the reference for each time-step t of the sequence, i.e., $\mathbf{e}_t = \hat{\mathbf{s}}_t - \mathbf{s}_t$. As is common in the ILC literature, we make use of the so-called *lifted system* formulation such that we can conveniently write the state evolution for one rollout using a single matrix/vector multiplication. Assuming zero initial state (which can always be done in the linear setting by just shifting the state by a constant offset), we obtain the following formulation

$$\mathbf{s} = \mathbf{F}\mathbf{a} + \mathbf{d}, \quad \text{with} \quad \mathbf{F} = \begin{bmatrix} 0 & \cdots & & \\ \mathbf{B} & 0 & & \\ \mathbf{AB} & \mathbf{B} & 0 & \\ \mathbf{A}^2\mathbf{B} & \mathbf{AB} & \mathbf{B} & \ddots \\ \vdots & & \ddots & \ddots \end{bmatrix} \in \mathbb{R}^{|\mathcal{S}|(T+1)\times|\mathcal{A}|T}. \tag{90}$$

Thus, we can write the state-error at the j-th iteration of ILC in the lifted representation as (recall that the disturbance $\mathbf{d}$ does not change across iterations)

$$\mathbf{e}^{(i)} = \hat{\mathbf{s}} - \mathbf{s}^{(i)} = \hat{\mathbf{s}} - \mathbf{F}\mathbf{a}^{(i)} - \mathbf{d}, \tag{91}$$

$$\mathbf{e}^{(i+1)} = \mathbf{e}^{(i)} - \mathbf{F}(\mathbf{a}^{(i+1)} - \mathbf{a}^{(i)}). \tag{92}$$

Now, the resulting optimization problem then becomes

$$\mathbf{a}_*^{(i+1)} = \underset{\mathbf{a}^{(i+1)}}{\arg\min}\, J\left(\mathbf{a}^{(i+1)}\right) \text{ with } J\left(\mathbf{a}^{(i+1)}\right) = \frac{1}{2}\|\mathbf{e}^{(i+1)}\|^2.$$

In order to be less sensitive to noise and the inherent stochasticity of real-world problems, one typically also adds a regularizing term that penalizes the changes in the input sequence. While this additional penalization term can slow down the learning process it makes it more robust by avoiding overcompensation to the disturbances. The full objective then becomes

$$J\left(\mathbf{a}^{(i+1)}\right) = \frac{1}{2}\|\mathbf{e}^{(i+1)}\|_{\mathbf{M}}^2 + \frac{1}{2}\|\mathbf{a}^{(i+1)} - \mathbf{a}^{(i)}\|_{\mathcal{W}}^2, \tag{93}$$

where we additionally added positive semi-definite cost matrices $\mathbf{M}, \mathcal{W}$ for the respective norms in order to facilitate tuning of the corresponding terms in the objective. Given the regularized cost function we obtain the optimal sequence of inputs at the next iteration as

$$\mathbf{a}_*^{(i+1)} = \mathbf{a}_*^{(i)} + \left(\mathbf{F}^\top \mathbf{M} \mathbf{F} + \mathcal{W}\right)^{-1} \mathbf{F}^\top \mathbf{M} \mathbf{e}^{(i)}. \tag{94}$$

D.2 Model-based RL to NO-ILC

Assumptions In order to show the equivalence of MBRL and NO-ILC we need to make some assumptions to the above stated optimization problem.

- No aleatoric uncertainty in the model, i.e., no transition noise $\omega_t = 0 \quad \forall t$.
- Typically in RL we assume the policy to be stationary, however, in this setting we will allow for non-stationary policies that are indexed by time t (the result will not necessarily depend on the state such that we essentially just obtain a feedforward control sequence. To include feedback one can always just combine the feedforward signal with a local controller that tracks the desired state/action trajectory).
- The reward is given as the negative quadratic error of the state w.r.t. a desired state trajectory, $r(\mathbf{s}_t, \mathbf{a}_t) = -\frac{1}{2}\|\hat{\mathbf{s}}_t - \mathbf{s}_t\|^2$
- Typically in RL we have constraints on the policy such that it does not change too much after every iteration, see e.g. TRPO, REPS, etc. While in the mentioned approaches, the policy are often constrained in terms of their parameterization vectors, we constrain it as $\|\pi_t^{(i+1)} - \pi_t^{(i)}\|^2 \leq \epsilon_\pi \quad \forall t$.
- Assume that the model is given by $\tilde{f}_t(\mathbf{s}, \mathbf{a}) = \mathbf{A}\mathbf{s} + \mathbf{B}\mathbf{a} + \mathbf{d}_t$, where $\mathbf{A}$ and $\mathbf{B}$ are fixed system matrices and $\mathbf{d}_t$ is a time-dependent offset that we learn.

The learned dynamics model Given state/input pairs of the i-th trajectory $\tau^{(i)} = \{(\mathbf{s}_t^{(i)}, \mathbf{a}_t^{(i)})\}_{t=0}^T$ from the true system, we can now improve our dynamics model. In particular, if we minimize the prediction error over $\tau^{(i)}$, we obtain

$$\mathbf{d}_t^{(i)} = \mathbf{s}_{t+1}^{(i)} - \left(\mathbf{A}\mathbf{s}_t^{(i)} + \mathbf{B}\mathbf{a}_t^{(i)}\right) \tag{95}$$

The resulting dynamics for the optimal control problem in Eq. (1) become

$$\tilde{f}_t^{(i)}(\mathbf{s}, \mathbf{a}) = \mathbf{s}_{t+1}^{(i)} + \mathbf{A}(\mathbf{s} - \mathbf{s}_t^{(i)}) + \mathbf{B}(\mathbf{a} - \mathbf{a}_t^{(i)}) \tag{96}$$

which are the error dynamics around the trajectory. Now in the noisy case, taking the last trajectory is not necessarily the best thing one can do. E.g., (Schöllig & D'Andrea, 2009) instead integrate the information of all past trajectories via Kalman-filtering. In the fully observed case, one way to think of this is as low-pass filtering $\mathbf{d}_t$ in order to account for the transition noise ω.

The resulting MBRL problem Now, let's plug in all assumptions into the MBRL problem and have a look at how to solve it.

$$\begin{aligned}
\pi_*^{(i+1)} = \underset{\pi=\{\pi_0,\dots,\pi_T\}}{\arg\min} \sum_{t=0}^{T} \frac{1}{2}\|\hat{\mathbf{s}}_t - \mathbf{s}_t\|^2 \\
\mathbf{s}_{t+1} = \mathbf{s}_{t+1}^{(i)} + \mathbf{A}(\mathbf{s} - \mathbf{s}_t^{(i)}) + \mathbf{B}(\mathbf{a} - \mathbf{a}_t^{(i)}) \\
\mathbf{a}_t = \pi_t \\
\|\pi_t^{(i)} - \pi_t\|^2 \leq \epsilon_\pi \quad \forall t
\end{aligned} \tag{97}$$

where we have flipped the reward's sign to transform it into a minimization problem. In the presented form, this optimization problem has a well-defined unique solution, however, it is a-priori not clear if the trust-region constraint is active for some time-steps. To facilitate an analytical solution to equation 97, we incorporate the constrain on the policy's stepsize by a soft-constraint such that

$$\begin{aligned}
\pi_*^{(i+1)} = \underset{\pi=\{\pi_0,\dots,\pi_T\}}{\arg\min} \sum_{t=0}^{T} \frac{1}{2}\|\hat{\mathbf{s}}_t - \mathbf{s}_t\|^2 + \frac{C_t^\pi}{2}\|\pi_t^{(i)} - \pi_t\|^2 \\
\mathbf{s}_{t+1} = \mathbf{s}_{t+1}^{(i)} + \mathbf{A}(\mathbf{s} - \mathbf{s}_t^{(i)}) + \mathbf{B}(\mathbf{a} - \mathbf{a}_t^{(i)}) \\
\mathbf{a}_t = \pi_t,
\end{aligned} \tag{98}$$

with C_t^π being constants that weight the respective trust-region terms.

Generally, the MBRL problem Eq. (2) cannot be solved analytically due to the (possibly highly non-linear, non-differentiable, etc.) reward signal and the need for propagating the (uncertain) dynamics model forwards in time. However, using the simplifying assumptions above, the reduced MBRL problem equation 98 can in fact be solved analytically. We can circumvent the equality constraints by predicting the state trajectory using the error corrected dynamics such that we obtain a lifted dynamics formulation similar to the analysis for ILC,

$$\mathbf{s}^{(i)} = \mathbf{F}\mathbf{a}^{(i)} + \mathbf{d}^{(i)}, \quad \text{with} \quad \mathbf{d}^{(i)} = \mathbf{s}^{(i)} - \mathbf{F}\mathbf{a}^{(i)}, \tag{99}$$

with $\mathbf{s}, \mathbf{a}$ denoting the stacked states and actions of the recorded trajectory. Using this notation, the optimization problem reduces to

$$\pi_*^{(i+1)} = \arg\min_{\pi} \frac{1}{2}\|\hat{\mathbf{s}} - \mathbf{s}^{(i)}\|^2 + \frac{1}{2}\|\pi^{(i)} - \pi\|^2_{\mathbf{C}^\pi}, \tag{100}$$

with $\mathbf{C}^\pi = \mathrm{diag}[C_0^\pi, \dots, C_H^\pi]$. By inserting equation 99 into equation 100 we obtain the closed-form solution as

$$\pi_*^{(i+1)} = \left(\mathbf{F}^\top\mathbf{F} + \mathbf{C}^\pi\right)^{-1}\mathbf{F}^\top\left(\hat{\mathbf{s}} - \mathbf{d}^{(i)}\right) = \pi_*^{(i)} + \left(\mathbf{F}^\top\mathbf{F} + \mathbf{C}^\pi\right)^{-1}\mathbf{F}^\top\left(\hat{\mathbf{s}} - \mathbf{s}^{(i)}\right), \tag{101}$$

which, clearly, is equivalent to equation 94 for $\mathbf{M} = \mathbf{I}$ and $\mathcal{W} = \mathbf{C}^\pi$.

D.3 Extensions

In the previous section, we analyzed the most basic setting for NO-ILC, i.e., linear dynamics, no transition noise in the dynamics and no state/input constraints. Some of these assumptions can easily be liftd to genearlized the presented framework.

Nonlinear Dynamics Instead of the system being defined by fixed matrices $\mathbf{A}, \mathbf{B}$, we can just linearize a non-linear dynamics model $f(\mathbf{s}, \mathbf{a})$ around the last state/input trajectory such that

$$\mathbf{A}_t^{(i)} = \left.\frac{\partial f}{\partial \mathbf{s}}\right|_{\mathbf{s}_t = \mathbf{s}_t^{(i)}, \mathbf{a}_t = \mathbf{a}_t^{(i)}}, \quad \mathbf{B}_t^{(i)} = \left.\frac{\partial f}{\partial \mathbf{a}}\right|_{\mathbf{s}_t = \mathbf{s}_t^{(i)}, \mathbf{a}_t = \mathbf{a}_t^{(i)}} \tag{102}$$

and the corresponding dynamics matrix for the lifted representation becomes (dropping the superscript notation indicating the iteration for clarity)

$$\mathbf{F} = \begin{bmatrix} 0 & \cdots & & \\ \mathbf{B}_0 & 0 & & \\ \mathbf{A}_0\mathbf{B}_0 & \mathbf{B}_1 & 0 & \\ \mathbf{A}_0\mathbf{A}_1\mathbf{B}_0 & \mathbf{A}_0\mathbf{B}_1 & \mathbf{B}_2 & \ddots \\ \vdots & & \ddots & \ddots \end{bmatrix} \in \mathbb{R}^{|\mathcal{S}|(T+1)\times|\mathcal{A}|T}. \tag{103}$$

State/Input Constraints Recall that we could solve the quadratic problems equation 93 and equation 98 analytically because we assumed no explicit inequality constraints on the state and inputs. In practice, however, both states and actions are limited by physical or safety constraints typically given by polytopes. While a closed-form solution is not readily available for this case, one can easily employ any numerical solver to deal with such constraints. See, e.g., `https://en.wikipedia.org/w/index.php?title=Quadratic_programming` for a comprehensive list of available solvers.

Stochastic Dynamics Schöllig & D'Andrea (2009) generalize the ILC setting by considering two separate sources of noise: 1) transition noise in the dynamics, i.e., $\mathbf{s}_{t+1} = f(\mathbf{s}_t, \mathbf{a}_t) + \omega_t^f$ as well as 2) varying disturbances, i.e., $\mathbf{d}^{(i+1)} = \mathbf{d}^{(i)} + \omega^d$. Based on this model, a Kalman-Filter in the *iteration-domain* is developed that estimates the respective random variables and the ILC scheme is adapted to account for the estimated quantities.

E Hyperparameter Settings

Below we list the most important hyperparameter settings.

Table 1: Hyperparameter settings for OPC (blue) and MBPO($\star$) (red) for results shown in Fig. 3. Note that the respective hyperparameters for each environment are shared across the different implementations, i.e., MuJoCo and PyBullet.

	HalfCheetah	Hopper	Walker2D	AntTruncatedObs
epochs	200	150	300	300
env steps per epoch	1000			
retain epochs	50 / 5	50	50	50 / 5
policy updates per epoch	40	20	20	20
model horizon	10			
model rollouts per epoch	100'000			
mix-in ratio	0.0			
model network	ensemble of 7 with 5 elites			
policy network	MLP with 2 hidden layers of size 64			

F Implementation and Computational Resources

Our implementation is based on the code from MBPO (Janner et al., 2019), which is open-sourced under the MIT license. All experiments were run on a HPC cluster, where each individual experiment used one nVidia V100 GPU and four Intel Xeon CPUs. All experiments (including early debugging and evaluations) amounted to a total of 84'713 hours, which corresponds to roughly 9.7 years if the jobs ran sequentially. Most of this compute was required to ensure reproducability (ten random seeds per job and ablation studies over the effects of parameters). Since the cluster is part of an overall carbon-neutral infrastructure, these experiments did not contribute to climate change.